Volume 4 | Issue 1 | June 2014 ISSN 2182-0287

Journal of Integrated OMICS

a methodological journal

JIOMICS

Journal of Integrated OMICS

Focus and Scope

Journal of Integrated OMICS, JIOMICS, provides a forum for the publication of original research papers, preliminary communications, technical notes and critical reviews in all branches of pure and applied "-omics", such as genomics, proteomics, lipidomics, metabolomics or metallomics. The manuscripts must address methodological development. Contributions are evaluated based on established guidelines, including the fundamental nature of the study, scientific novelty, and substantial improvement or advantage over existing technology or method. Original research papers on fundamental studies, and novel sensor and instrumentation development, are especially encouraged. It is expected that improvements will also be demonstrated within the context of (or with regard to) a specific biological question; ability to promote the analysis of molecular mechanisms is of particular interest. Novel or improved applications in areas such as clinical, medicinal and biological chemistry, environmental analysis, pharmacology and materials science and engineering are welcome.

Editors-in-Chief

Regional editors

Asia

Australia and New Zealand

Europe

North America

Australia and New Zealand

ARC Centre of Excellence in Plant Energy Biology & Centre for Comparative Analysis of Biomolecular Networks (CABiN), University of Western Australia, Perth, Australia

Peter Hoffmann
Institute for Photonics & Advanced Sensing (IPAS), School of Chemistry and Physics, University of Adelaide, Australia

Stefan Clerens
Protein Quality &Function, AgResearch Ltd Christchurch, New Zealand

Peter Solomon
Research School of Biology College of Medicine, Biology and Environment, Australian National University, Australia

Phoebe Chen
Department of Computer Science and Computer Engineering, La Trobe University, Melbourne, Australia

Richard Christopherson
School of Molecular Bioscience, University of Sydney, Australia

Sham Nair
Department of Biological Sciences, Faculty of Science, Macquarie University, NSW, Australia

Sylvia Urban
School of Applied Sciences (Discipline of Applied Chemistry), RMIT University, Melbourne, Victoria, Australia

Valerie Wasinger
Bioanalytical Mass Spectrometry Facility, Mark Wainwright Analytical Centre, University of NSW, Australia

Wujun Ma
Centre for Comparative Genomics, Murdoch University, Australia

Yin Xiao
Institute of Health and Biomedical Innovation, Queensland University of Technology, Australia

EUROPE

AhmetKoc, PhD
Izmir Institute of Technology, Department of Molecular Biology & Genetics, Urla, İzmir, Turkey

Alejandro Gella
Department of Basic Sciences, Neuroscience Laboratory, Faculty of Medicine and Health Sciences, Universitat Internacional de Catalunya,
Sant Cugat del Vallès-08195, Barcelona, Spain

Alessandro Pessione
Università degli Studi di Torino, Italy

Alexander Scherl
Proteomics Core Facility, Faculty of Medicine, University of Geneva, Geneva, Switzerland

Alfio Ferlito
ENT Clinic, University of Udine, Italy

Almudena Fernández Briera
Dpt. Biochemistry Genetics and Immunology, Faculty of Biology –University of Vigo, Spain

Alfonsina D'Amato
Politecnico di Milano, Department of Chemistry, Materials and Chemical Engineering "GiulioNatta", Italy

Alfred Vertegaal
Molecular Cell Biology, Leiden University Medical Center, The Netherlands

Ali Mobasheri
School of Veterinary Medicine and Science, Faculty of Medicine and Health Sciences, University of Nottingham, Sutton Bonington Campus, Sutton Bonington, Leicestershire, United Kingdom

Andre Almeida
Instituto de Tecnología Química e Biológica, Universidade Nova de Lisboa, Portugal

Andrea Matros
Leibniz Institute of Plant Genetics and Crop Plant Research (IPK-Gatersleben), Gatersleben, Germany

Andrei Turtoi
University of Liege, Metastasis Research Laboratory, GIGA-Cancer Bât. B23, Belgium

Angelo D'Alessandro
Università degli Studi della Tuscia, Department of Ecological and Biological Sciences, Viterbo, Italy

Angelo Izzo
Department of Experimental Pharmacology, University of Naples Federico II, Naples, Italy

Antonio Gnoni
Department of Medical Basic Sciences, University of Bari "Aldo Moro", Bari, Italy

Ana Maria Rodríguez-Piñeiro
Institute of Biomedicine, University of Gothenburg, Sweden

Ana Varela Coelho
Instituto de Tecnologia Química e Biológica (ITQB) Universidade Nova de Lisboa (UNL), Portugal

Anna Maria Timperio
Dipartimento Scienze Ambientali Università della Tuscia Viterbo, Italy

André Nogueira Da Costa
Molecular Carcinogenesis Group, Section of Mechanisms of Carcinogenesis International Agency for Research on Cancer - World Health Organization (IARC-WHO), Lyon, France

Andreas Boehm
Steigerfurtweg 8a, D-97084 Würzburg, Germany

Andrea Scaloni
Proteomics and Mass Spectrometry Laboratory, ISPAAM, National Research Council, via Argine 1085, 80147 Napoli, Italy

Andreas Tholey
Division for Systematic Proteome Research, Institute for Experimental Medicine, Christian-Albrechts-University, Germany

Angel Manteca
Departamento de Biologia Funcional and IUBA, Facultad de Medicina, Universidad de Oviedo, Spain

Angel P. Diz
Department of Biochemistry, Genetics and Immunology, Faculty of Biology, University of Vigo, Spain

Angela Bachi
Mass Spectrometry Unit DIBIT, San Raffaele Scientific Institute, Milano, Italy

Angela Chambery
Department of Life Science, Second University of Naples, Italy

Anna-Irini Koukkou
University of Ioannina, Department of Chemistry, Biochemistry Laboratory, Greece

António Sebastião Rodrigues
Departamento de Genética, Faculdade de Ciências Médicas, Universidade Nova de Lisboa,Portugal

Arkadiusz Kosmala
Laboratory of Cytogenetics and Molecular Biology, Institute of Plant Genetics, Polish Academy of Sciences, Poland

Arzu Umar
Department of Medical Oncology, Laboratory of Breast Cancer Genomics and Proteomics, Erasmus Medical Center Rotterdam Josephine Nefkens Institute, Rotterdam, The Netherlands

Baggerman Geert
ProMeta, Interfacultary Center for Proteomics and Metabolomics, Leuven,

JOURNAL OF INTEGRATED OMICS

A methodological Journal

CONTENTS OF VOLUME 4 | ISSUE 1 | JUNE 2014

POINT OF VIEW

ORIGINAL ARTICLES

JOURNAL OF INTEGRATED OMICS
A METHODOLOGICAL JOURNAL
HTTP://WWW.JIOMICS.COM

POINT OF VIEW | DOI: 10.5584/jiomics.v4i1.165

Differential proteomics has emerged as a tool to understand carbapenem resistance in *Acinetobacter baumannii*

Vishvanath Tiwari*

Department of Biochemistry, Central University of Rajasthan, Ajmer, Rajasthan, 305801, India.

Received: 05 April 2014 **Accepted:** 30 June 2014 **Available Online**: 30 June 2014

Acinetobacter baumannii is one of the opportunistic pathogens described by Infectious Disease Society of America [1]. Due to its pathogenicity, it is grouped into ESKAPE pathogens, a group of pathogens causing hospital-acquired infections [2-3]. *Acinetobacter baumannii* has emerged as a threat to soldiers, wounded during military operations in Iraq and Afghanistan [4-5], and also isolated from natural resources [6]. It causes pneumonia, respiratory infections and urinary tract infections. It can grow on artificial surfaces, utilize ethanol as a carbon source [7], resist desiccation, survive at various temperatures, and pH conditions [8]. These abilities make it a 'lethal' pathogen. Prevalence of *Acinetobacter baumannii* in clinical setup increases gradually [9]. Commonly prescribed drug against *A. baumannii* are carbapenems which belongs to the β-lactam group of antibiotics [10]. *Acinetobacter baumannii* has emerged resistance against carbapenem which is a significant health problem and responsible for high morbidity & mortality [11]. This makes it one of the major health concerns [9, 12-13].

Proteomics emerged as a tool to study the differential proteome under diverse conditions. With the development of methods used in the proteomics, a considerable progress has been made in the recent years in the field of differential proteomics. Various methods have been employed to study the differential proteomics. These methods include gel based methods like DIGE [14], gel free methods like ICAT [15], iTRAQ [16], SILIC [17], ICPL [18], and mass spectrometry based methods like SRM [19]. Isotope labels can be incorporated into peptides chemically or enzymatically or metabolically or inverse labeling-based [20]. In label free proteomics mass spectrometer recognizes the mass difference and their quantification are achieved by comparing their respective signal intensities.

Differential proteomics between wild type and carbapenem resistance strain of *Acinetobacter baumannii* was first reported by the Vila and colleagues [21]. Similarly, Siroy et al also performed the differential global comparison of the membrane sub-proteomes of multidrug-resistant *Acinetobacter baumannii* strain and a reference strain [22]. Using differential proteomics approach, Soares et al showed that *Acinetobacter baumannii* displays a robust and versatile metabolism [23]. With the help of differential outer membrane proteomics, Kwon et al, studied the secretion of outer membrane vesicles (OMVs) from a clinical *A. baumannii* isolate and analysed the comprehensive proteome of *A. baumannii*-derived OMVs [24]. Similarly, high-end isoelectric point (pH 6-11) differential proteome analysis of *Acinetobacter radioresistens* S-13 reveals that envelope stress responses can be induced by aromatic compounds [25]. Biofilm formation is one of the important causes for the persistence of *Acinetobacter baumannii* on the surface of host epithelial cells. Cabral et al, performed differential proteomics of *Acinetobacter* cultured in three different conditions (exponential, late stationary phase and biofilms stage) and they also checked the effects of biofilm inhibitory compound (salicylate) on the biofilm formation. This multiple-approach strategy showed a unique lifestyle of *A. baumannii* involved in biofilms formation [26]. Yun et al, performed differential quantitative proteomic analysis of cell wall and plasma membrane fractions from multidrug-resistant *Acinetobacter baumannii* and reported that carbapenem induces the expression of resistance-nodulation-cell division transporters, protein kinases and suppress outer

***Corresponding author:** Vishvanath Tiwari, Department of Biochemistry, Central University of Rajasthan, Ajmer, Rajasthan, 305801, India; Phone No.: + 91-1463-238652; Fax No: + 91-1463-238722; E-mail address: vishvanath7@yahoo.co.in

membrane proteins expression [27]. Lee et al explain the mechanism of hetero-resistance induced by imipenem (a member of carbapenem group) in the multidrug resistance *Acinetobacter baumannii* [28]. Rajeswari et al showed the importance of outer membrane in the carbapenem resistance using differential outer membrane proteomics of carbapenem resistance strain of *Acinetobacter baumannii* [29]. Tiwari et al identified the importance of the metabolism in the carbapenem resistance of *Acinetobacter* using differential inner membrane proteomics [13]. Role of iron in the survival of ATCC strain and carbapenem resistance strain of *Acinetobacter baumannii* in human host has also been studied using differential proteomics [30-31]. Proteome of the human host also changed during *Acinetobacter baumannii* infection. Soares et al, identified alterations in the plasma proteome of individuals infected with *Acinetobacter baumannii* as compared to healthy controls using DIGE based differential proteomic approach [32].

These updates show that differential proteomics has now emerged as an important tool to understand the mechanism of carbapenem resistance in *Acinetobacter baumannii*. Differential proteomics also helps to understand the role of different environments/conditions in the survival of *Acinetobacter baumannii* and its adaptation as a notorious pathogen.

References

[1] H.W. Boucher, G.H. Talbot, J.S. Bradley, J.E. Edwards, D. Gilbert, L.B. Rice, M. Scheld, B. Spellberg, J. Bartlett, Clinical infectious diseases : an official publication of the Infectious Diseases Society of America, 48 (2009) 1-12. doi: 10.1086/595011

[2] R.M. Klevens, J.R. Edwards, F.C. Tenover, L.C. McDonald, T. Horan, R. Gaynes, Clinical infectious diseases : an official publication of the Infectious Diseases Society of America, 42 (2006) 389-391. doi: 10.1086/499367

[3] H.W. Boucher, G.R. Corey, Clinical infectious diseases : an official publication of the Infectious Diseases Society of America, 46 Suppl 5 (2008) S344-349. doi: 10.1086/533590

[4] K.A. Davis, K.A. Moran, C.K. McAllister, P.J. Gray, Emerging Infectious Diseases, 11 (2005) 1218-1224. doi: 10.3201/1108.050103

[5] C. Camp, O.L. Tatum, Laboratory Medicine, 41 (2010) 649-657. doi: 10.1309/lm90ijnddwri3re

[6] M. Kempf, J.M. Rolain, G. Diatta, S. Azza, B. Samb, O. Mediannikov, A. Gassama Sow, S.M. Diene, F. Fenollar, D. Raoult, PloS one, 7 (2012) e39495. doi: 10.1371/journal.pone.0039495

[7] S. Navon-Venezia, R. Ben-Ami, Y. Carmeli, Curr Opin Infect Dis, 18 (2005) 306-313. doi: 10.1097/01.qco.0000171920.44809.f0

[8] E. Bergogne-Berezin, K.J. Towner, Clinical microbiology reviews, 9 (1996) 148-165. doi:

[9] V. Tiwari, A. Kapil, R.R. Moganty, Microbial pathogenesis, 53 (2012) 81-86. doi: 10.1016/j.micpath.2012.05.004

[10] P.M. Hawkey, A.M. Jones, The Journal of antimicrobial chemotherapy, 64 Suppl 1 (2009) i3-10. doi: 10.1093/jac/dkp256

[11] D.M. Sengstock, R. Thyagarajan, J. Apalara, A. Mira, T. Chopra, K.S. Kaye, Clinical infectious diseases : an official publication of the Infectious Diseases Society of America, 50 (2010) 1611-1616. doi: 10.1086/652759

[12] V. Tiwari, I. Nagpal, N. Subbarao, R.R. Moganty, Journal of molecular modeling, 18 (2012) 3351-3361. doi: 10.1007/s00894-011-1346-3

[13] V. Tiwari, J. Vashistt, A. Kapil, R.R. Moganty, PloS one, 7 (2012) e39451. doi: 10.1371/journal.pone.0039451

[14] M. Unlu, M.E. Morgan, J.S. Minden, Electrophoresis, 18 (1997) 2071-2077. doi: 10.1002/elps.1150181133

[15] S.P. Gygi, B. Rist, S.A. Gerber, F. Turecek, M.H. Gelb, R. Aebersold, Nature biotechnology, 17 (1999) 994-999. doi: 10.1038/13690

[16] C.S. Gan, P.K. Chong, T.K. Pham, P.C. Wright, Journal of proteome research, 6 (2007) 821-827. doi: 10.1021/pr060474i

[17] S.E. Ong, Molecular & Cellular Proteomics, 1 (2002) 376-386. doi: 10.1074/mcp.M200025-MCP200

[18] J. Kellermann, Methods in molecular biology, 424 (2008) 113-123. doi: 10.1007/978-1-60327-064-9_10

[19] S. Elschenbroich, T. Kislinger, Molecular bioSystems, 7 (2011) 292-303. doi: 10.1039/c0mb00159g

[20] H.M. Santos, D. Glez-Pena, M. Reboiro-Jato, F. Fdez-Riverola, M.S. Diniz, C. Lodeiro, J.L. Capelo-Martinez, Electrophoresis, 31 (2010) 3407-3419. doi: 10.1002/elps.201000251

[21] S. Marti, J. Sanchez-Cespedes, E. Oliveira, D. Bellido, E. Giralt, J. Vila, Proteomics, 6 Suppl 1 (2006) S82-87. doi: 10.1002/pmic.200500323

[22] A. Siroy, P. Cosette, D. Seyer, C. Lemaitre-Guillier, D. Vallenet, A. Van Dorsselaer, S. Boyer-Mariotte, T. Jouenne, E. De, Journal of proteome research, 5 (2006) 3385-3398. doi: 10.1021/pr060372s

[23] N.C. Soares, M.P. Cabral, J.R. Parreira, C. Gayoso, M.J. Barba, G. Bou, Proteome science, 7 (2009) 37. doi: 10.1186/1477-5956-7-37

[24] S.O. Kwon, Y.S. Gho, J.C. Lee, S.I. Kim, FEMS microbiology letters, 297 (2009) 150-156. doi: 10.1111/j.1574-6968.2009.01669.x

[25] R. Mazzoli, P. Fattori, C. Lamberti, M.G. Giuffrida, M. Zapponi, C. Giunta, E. Pessione, Molecular bioSystems, 7 (2011) 598-607. doi: 10.1039/c0mb00112k

[26] M.P. Cabral, N.C. Soares, J. Aranda, J.R. Parreira, C. Rumbo, M. Poza, J. Valle, V. Calamia, I. Lasa, G. Bou, Journal of proteome research, 10 (2011) 3399-3417. doi: 10.1021/pr101299j

[27] S.H. Yun, C.W. Choi, S.O. Kwon, G.W. Park, K. Cho, K.H. Kwon, J.Y. Kim, J.S. Yoo, J.C. Lee, J.S. Choi, S. Kim, S.I. Kim, Journal of proteome research, 10 (2011) 459-469. doi: 10.1021/pr101012s

[28] H.Y. Lee, C.L. Chen, S.B. Wang, L.H. Su, S.H. Chen, S.Y. Liu, T.L. Wu, T.Y. Lin, C.H. Chiu, International journal of antimicrobial agents, 37 (2011) 302-308. doi: 10.1016/j.ijantimicag.2010.12.015

[29] J. Vashist, V. Tiwari, A. Kapil, M.R. Rajeswari, Journal of proteome research, 9 (2010) 1121-1128. doi: 10.1021/pr9011188

[30] C.C. Nwugo, J.A. Gaddy, D.L. Zimbler, L.A. Actis, Journal of proteomics, 74 (2011) 44-58. doi: 10.1016/j.jprot.2010.07.010

[31] V. Tiwari, R.R. Moganty, Journal of Proteomics & Bioinformatics, 06 (2013) 125-131. doi: 10.4172/jpb.1000270

[32] A.J. Soares, M.F. Santos, M.R. Trugilho, A.G. Neves-Ferreira, J. Perales, G.B. Domont, Journal of proteomics, 73 (2009) 267-278. doi: 10.1016/j.jprot.2009.09.010

JOURNAL OF INTEGRATED OMICS
A METHODOLOGICAL JOURNAL
HTTP://WWW.JIOMICS.COM

ORIGINAL ARTICLE | DOI: 10.5584/jiomics.v4i1.157

Subtoxic concentrations of benzo[*a*]pyrene induce metabolic changes and oxidative stress in non-activated and affect the mTOR pathway in activated Jurkat T cells

Sven Baumann[1,#], Maxie Rockstroh[2,#], Jörg Bartel[3], Jan Krumsiek[3], Wolfgang Otto[2], Harald Jungnickel[4], Sarah Potratz[4], Andreas Luch[4], Edith Wilscher[5], Fabian J. Theis[3,6], Martin von Bergen[1,2,7], Janina M. Tomm[2,*]

[1]Department of Metabolomics, Helmholtz-Centre for Environmental Research - UFZ, Permoser Str. 15, 04318 Leipzig, Germany; [2]Department of Proteomics, Helmholtz-Centre for Environmental Research - UFZ, Permoser Str. 15, 04318 Leipzig, Germany; [3]Institute of Bioinformatics and Systems Biology, Helmholtz Zentrum München, Ingolstädter Landstr. 1, 85764 Neuherberg, Germany; [4]Department of Product Safety, German Federal Institute for Risk assessment (BfR), Max-Dohrn Strasse 8-10, 10589 Berlin, Germany; [5]Interdisciplinary Centre for Bioinformatics, University of Leipzig, Härtelstr. 16-18, 04107 Leipzig, Germany; [6]Institute for Mathematical Sciences, TU München, Boltzmannstr. 3, 85747 Garching, Germany; [7]Aalborg University, Department of Biotechnology, Chemistry and Environmental Engineering, Aalborg University, Sohngaardsholmsvej 49, DK-9000 Aalborg, Denmark. [#] *contributed equally*

Received: 09 October 2013 **Accepted:** 26 December 2013 **Available Online**: 17 February 2014

Abstract

Recent studies have shown that aromatic compounds, such as B[*a*]P, influence the immune system even at low concentrations. Although the activation of immune cells is the first and thereby pivotal step in the immunological cascade, the current knowledge about the impact of environmental pollutants on this process is quite limited. Therefore, we investigated the effect of a subtoxic B[*a*]P concentration (50 nM) on the proteome and the metabolome of non-activated and activated Jurkat T cells. The GeLC-MS/MS analysis yielded 2624 unambiguously identified proteins. In addition to typical regulatory pathways associated with T cell activation, pathway analysis by Ingenuity IPA revealed several metabolic processes, for instance purine and pyruvate metabolism. The activation process seems to be influenced by B[*a*]P suggesting an important role of the mTOR pathway in the cellular adaptation. B[*a*]P exposure of non-activated Jurkat cells induced signaling pathways such as protein ubiquitination and NRF2 mediated oxidative stress response as well as metabolic adaptations involving pyruvate, purine and fatty acid metabolism. Thus, we validated the proteome results by determining the concentrations of 183 metabolites with FIA-MS/MS and IC-MS/MS. Furthermore, we were able to show that Jurkat cells metabolize B[*a*]P to B[*a*]P-1,6-dione. The combined evaluation of proteome and metabolome data with an integrated, genome-scale metabolic model provided novel systems biological insights into the complex relation between metabolic and proteomic processes in Jurkat T cells during activation and subtoxic chemical exposure.

Keywords: benzo[*a*]pyrene; antioxidant response element; *Jurkat T cell; activation; LC-MS/MS; Biocrates*.

Abbreviations

AhR: aryl hydrocarbon receptor; **APC**: antigen presenting cell; **APCI**: atmospheric-pressure chemical ionization; **ARE**: antioxidant response element; **B[*a*]P**: benzo[*a*]pyrene; **FDR**: false discovery rate; **FIA-MS/MS**: flow injection assay mass spectrometry; **GeLC-MS/MS**: 1D PAGE protein separation followed by liquid chromatography-tandem mass spectrometry; **IC-MS/MS**: ion chromatography coupled to mass spectrometry; **IL-2**: interleukin-2; **mTOR**: mammalian target of rapamycin; **NRF2**: nuclear factor erythroid 2-related factor 2; **PI**: propidium iodide; **XRE**: xenobiotic response element.

***Corresponding author:** Janina M. Tomm, Department of Proteomics, Helmholtz-Centre for Environmental Research - UFZ, Permoser Str. 15, 04318 Leipzig, Germany. Phone number: +49-0341-2351819; Fax number: +49-0341-2351786; E-mail address: janina.tomm@ufz.de

1. Introduction

T cell development, subset lineage specification, survival and death are dependent on the initial step of T cell receptor activation [1]. Many major milestones in understanding this process originate from experiments with transformed T cell lines, such as Jurkat T cells [2]. Only very few proteomic studies focus on the activation of Jurkat cells. Those experiments either established new proteomic methods [3], or focused on detecting the protein composition of lipid rafts [4] and on elucidating general signaling pathways [5]. Thus the consequences of the different signaling patterns on the proteome are not well characterized yet. Furthermore, metabolomic processes are known to play an important role in T cell activation and differentiation [6].

The specific outcome of T cell stimulation is based on the integration of complex signals from the cellular microenvironment, which can be affected by environmental pollutants, such as B[*a*]P. Earlier findings showed that B[*a*]P and its metabolites influence cell mediated as well as humoral immunity [7] at rather low concentrations, but the mechanisms remain largely unknown. The chemical and biological inert B[*a*]P can be metabolically activated in the cell by three different pathways - the diol epoxide, the *o*-quinone and the radical cation pathway [8]. The cytochromes P4501A1/1B1, which are involved in the diol epoxide and *o*-quinone pathway, can be induced via AhR signaling [9]. Although it is known that some T lymphocytes, such as Th17 cells, express AhR at high levels, most of the other T helper cell subpopulations are reported to lack AhR [10, 11]. This led to the hypothesis of AhR-independent pathways causing the observed effects. One possible pathway is the activation of the transcription factor NRF2. Electrophilic compounds, such as those generated in the course of B[*a*]P transformation, directly or indirectly cause oxidative stress. This stress leads to the oxidation of the Kelch-like ECH-associated protein 1 (KEAP1), which then loses its ability to sequester NRF2 in the cytosol. After dissociation from KEAP1, NRF2 translocates into the nucleus and binds to ARE-elements. This binding activates the transcription of phase II detoxifying enzymes [12] and other proteins [13] that are partly redundant and partly complementary to the effects of the AhR signaling pathway.

In our previous experiments [14] and other studies about the effects of B[*a*]P on the proteome [15] mostly gel-based methods were applied. As the number of regulated proteins identified and quantified with this method is quite limited, we chose a GeLC-MS/MS setup this time. We were able to increase the number of identified and quantified proteins up to 2624 in total in comparison to 608 quantified and 112 identified protein spots in the previous study. Furthermore, our recent work showed strong evidence for alterations in metabolic pathways caused by B[*a*]P exposure in activated Jurkat T cells, especially in the glutamine metabolism [14]. Hence, we intensively examined the metabolomic changes with the help of FIA-MS/MS and IC-MS/MS in addition to proteomic alterations. We were able to analyze 183 metabolites in contrast to only 2 metabolites in the earlier study. Moreover, we investigated the effect of activation itself and the influence of B[*a*]P to gain deeper insights into the activation process and the toxicological effects of B[*a*]P on it. The proteome data were used to identify the involved cellular and metabolic pathways, which were verified and complemented by Western blotting and metabolomic analysis. Additionally, we analyzed the biotransformation of B[*a*]P in this cell line.

2. Material and Methods

2.1. *Activation and B[a]P exposure*

Jurkat T cells (clone E6-1, TIB-152, LGC Promochem, Wesel, Germany) were maintained as described earlier [16]. Four different treatments were performed: incubation with DMSO (control); exposure to B[*a*]P (B[*a*]P); activation and incubation with DMSO (activated); activation and exposure to B[*a*]P (activated + B[*a*]P). At first the cells were activated with 750 ng/ml ionomycin (IO) and 10 ng/ml phorbol-12-myristat-13-acetate (PMA) for 4 h or left untreated for the non-activated samples. Afterwards the cells were collected and resuspended in fresh medium supplemented with 50 nM B[*a*]P (all Sigma-Aldrich, Steinheim, Germany) dissolved in dimethylsulfoxide (DMSO; Applichem, Darmstadt, Germany) or fresh medium supplemented only with DMSO (for samples without B[*a*]P exposure). After B[*a*]P exposure for 24 h, all cells and supernatants were collected for all further analysis (except B[*a*]P metabolite analysis). All experiments were carried out in triplicates.

2.2. *Determination of cell viability and activation status*

After 4 h of activation and the following 24 h B[*a*]P exposure the viability and the activation status of the cells was analyzed by flow cytometry. 1 µl propidium iodide (Miltenyi Biotech, Bergisch Gladbach, Germany) or 1 µl annexin V-FITC (Abcam plc, Cambridge, UK) were used to stain $1x10^5$ cells for 5 min at room temperature to verify the viability of the cells. In order to determine the cell activation, $1x10^5$ cells were stained with 1 µl anti-CD25-PE (Miltenyi Biotech, Bergisch Gladbach, Germany) or 1 µl anti-CD69-PE (Immunotech, Marseille, France) at 4°C. The samples were measured on a FACSCalibur (Becton-Dickinson, Erembodegem, Belgium). The cell viability was assessed for all cells, whereas the activation markers were evaluated only for viable cells (based on cell size).

2.3. *Cell fractionation, 1D-SDS-PAGE and Western blotting*

For analysis with GeLC-MS/MS the cells were fractionated with the Qproteome Cell Compartment Kit (Qiagen, Hilden, Germany) as described previously [16].

A salt fractionation with increasing KCl concentrations (10, 200 and 400 mM) and different centrifugation steps with increasing velocity was performed to verify the expression of

NF-κB1 and phospho-eIF2α in different cellular compartments. All KCl buffers contained 10 mM HEPES, pH 7.4; 1.5 mM $MgCl_2$; 339 mM sucrose; 10% glycerol; 1x protease inhibitor (Roche, Mannheim, Germany) and the additions stated in brackets. After activation and B[*a*]P exposure the cells were washed two times with cold 1x PBS (5 min; 300 x g; 4°C). The volume of the packed cells was determined and the triple of that volume was used for all following buffers. The pellet was resuspended in 10 mM KCl buffer (0.1% Triton X-100; 10 mM KCl) and incubated on ice for 5 min. After centrifugation at 1,300 x g and 4°C for 5 min the supernatant was saved as 10 mM fraction (cytoplasm) and the pellet was solved in 200 mM KCl buffer (200 mM KCl) and incubated at 4°C for 60 min shaking at 850 rpm. The suspension was centrifuged at 15,000 x g and 4°C for 15 min and the supernatant was saved as 200 mM fraction. The pellet was dissolved in 400 mM KCl buffer (400 mM KCl) and again incubated at 4°C for 60 min shaking at 850 rpm. After a last centrifugation step at 15,000 x g and 4°C for 15 min the supernatant contained the 400 mM fraction. The pellet was resuspended in Benzonase buffer (50 mM Tris-HCl; 1 mM $MgCl_2$; 1x protease inhibitor) and 1 µl Benzonase (Novagen) was added. This mixture was incubated at 37°C for about 1.5 h with shaking (400 rpm) until the big clump of DNA and proteins was homogenized and saved as pellet fraction (nucleus). The protein content of all fractions was determined using the Pierce 660 nm Protein Assay (Thermo Fisher Scientific, Bonn, Germany) according to the manufacturer's instruction, but with 5 µl of all samples and standards. 30 µg of the indicated fractions from the salt fractionation were analyzed with immunoblots as described elsewhere [17]. Anti-NF-κB1 (1:200, #3035), anti-H2A (1:1000, #2578), anti-phospho-eIF2α (1:200, #3398, all Cell Signaling Technology) and anti-PSMA4 (1:100, H-128, Santa Cruz Biotechnology) were used as primary antibodies. Chemiluminescence signal was measured using Pierce ECL Western Blotting Substrate (Thermo Fisher Scientific, Bonn, Germany) on a FluorChem 8900 (Alpha Innotech). Immunoblot signals were quantified with ImageJ software (http://rsbweb.nih.gov/ij/). The content of cytoplasmic and nuclear proteins was normalized using the signals of the two 'housekeeping' proteins PSMA4 or H2A, respectively.

2.4. *Sample preparation, LC-MS/MS analysis and data processing*

The proteins were digested and analyzed with GeLC-MS/MS as described elsewhere [16]. The MS/MS data were evaluated with MaxQuant (version 1.2.2.5) using the human Uniprot database (version 11/16/2011). Carbamidomethylation of cysteine was specified as a fixed modification, whereas oxidation of methionine and acetylation of the protein N-terminus were specified as variable modifications. Peptide and protein FDR were set to 1%. A minimum of two peptides with at least one unique peptide was used for protein identification. Proteins were quantified by label-free quantification with a minimum ratio count of 1 and a match between runs time window of 4 min. The overall label-free quantification intensity of each sample was normalized to the average overall label-free quantification intensity of all samples from one fraction. Only proteins found in at least two of three replicates in all four different treatments were further analyzed. Fold changes were calculated between the label-free quantification intensities from the different treatments and a Student's t-test was conducted on the log2 label-free quantification intensities for each comparison. Proteins with a p-value less than 0.05 and an average linear fold change higher than 1.5 were considered as significantly regulated.

2.5. *Extraction and measurement of cellular metabolites*

Concentrations of 163 metabolites from cell lysates were determined using a targeted metabolic approach with the AbsoluteIDQ p150 kit (BIOCRATES Life Sciences AG, Innsbruck, Austria) as described earlier [18]. Briefly, extraction of cell pellets was carried out using 300 µl methanol/water (1/1 v/v) and ultrasonic homogenization for 2 min on ice. Samples were centrifuged and 30 µl of supernatants were prepared according to the manufacturer's protocol [19]. FIA-MS/MS analyses were carried out on an Agilent 1100 series binary HPLC system (Agilent Technologies, Waldbronn, Germany) coupled to an 4000 QTrap mass spectrometer (AB Sciex, Concord, Canada) equipped with a TurboIon spray source. Quantification was achieved by positive and negative multiple reaction monitoring (MRM) detection in combination with the use of stable isotope-labeled and other internal standards. Data evaluation for quantification of metabolite concentrations was performed with the MetIQ™ software package.

For IC-MS/MS analysis, extracts were diluted ten-fold in Milli-Q water and measured on an ICS-5000 (Thermo Fisher Scientific, Dreieich, Germany) coupled to an API 5500 QTrap (AB Sciex). Separation was achieved on an IonPac AS11-HC column (2 x 250mm, Thermo Fisher Scientific) with an increasing potassium hydroxide gradient. MS analysis was performed in MRM mode using negative electrospray ionization and included organic acids, carbohydrates and nucleotides involved in central metabolite pathways.

2.6. *Measurement of B[a]P and B[a]P metabolites*

Cell pellets from Jurkat T cells exposed to 50 nM, 5 µM, 10 µM and 50 µM B[*a*]P for 4 h and 24 h, were dissolved in 1 ml ethylacetate, homogenized and internal standards were added and vortexed for 2 min. The ethylacetate phase was evaporated and the residue was re-suspended in 50 µl methanol:water (1/1 v/v). 10 µl were injected into a Shimadzu LC-20 HPLC system (Shimadzu, Duisburg, Germany) coupled to an API 4000 QTrap mass spectrometer (AB Sciex). Chromatography was performed on an Envirosep PP column (125 mm × 2 mm, 5 µm particle size, Phenomenex, Aschaffenburg, Germany) at 20°C with a flow rate of 0.2 ml/

min using 5 mM ammonium acetate in methanol:water (1/1 v/v) and 5 mM ammonium acetate in methanol for gradient elution within 25 min. Analysis was conducted in the APCI mode (source temperature: 350°C) under MRM mode for quantification.

2.7. *Pathway analysis*

Proteins quantified in at least two out of the three replicates in all four treatments were analyzed further using IPA Ingenuity build 131235, version 11904312 (Ingenuity Systems, Inc., Redwood City, CA, USA). The analysis was performed using the preset parameters (see supplement) and excluding pathways related to cardiovascular signaling as well as neurotransmitter and other nervous system signaling.

2.8. *Metabolic network construction*

In order to integrate the content of the KEGG, EHMN and BiGG databases, identical compounds were merged based on common identifiers like KEGG IDs. Thereby, additional information on enzymes catalyzing identical biochemical reactions from the individual databases was preserved. Database-specific compounds that could not be mapped were built into the integrated metabolic network according to the reactions they participate in. The largest connected component of the integrated network was used for further analysis. It consisted of 3657 metabolite nodes and 5389 reaction nodes, and 45696 edges between the two node partitions.

2.9. *Subgraph extraction by k-walks algorithm*

In order to infer the relationships between the differentially regulated entities and to identify the metabolic pathways that are most relevant for the experimental condition, we mapped the lists of significantly regulated proteins from all three fractions as well as metabolites onto the integrated network. Given these significantly regulated species as seed nodes, the k-walks algorithm and a minimal threshold as described in [20] were applied to extract meaningful subgraphs from the metabolic network.

3. Results and discussion

3.1. *Influence of B[a]P exposure on the cell viability and activation status*

The cell viability and activation status of the Jurkat T cells was assessed after activation and B[*a*]P exposure by FACS measurement (Figure 1). In control cells and B[*a*]P treated cells, between 7 and 8% were annexin V or PI positive. Activated cells showed a fraction of 28% PI positive and 34% annexin V positive cells. In both, activated and non-activated cells, there was no difference in viability due to B[*a*]P exposure, indicating that a concentration of 50 nM B[*a*]P is not cytotoxic for Jurkat T cells within the time of exposure (24 h). The higher amount of apoptotic cells in the activated samples can be attributed to the known phenomenon of activation-induced cell death, a specific form of apoptosis initiated in previously activated T cells following restimulation via the T cell receptor complex [20]. A comparable number of around 30% apoptotic cells was measured by Chwae et al. in Jurkat T cells after stimulation with 100 ng/ml PMA and 1 g/ml ionomycin for 24 h [21].

Nearly all activated cells (with or without B[*a*]P exposure) were positive for the early activation marker CD69. In contrast, around 37% and 34% of the cells were CD25 positive in the activated and activated plus B[*a*]P exposed cells, respectively. For both activation markers, the amount of positive cells in non-activated and activated cells was slightly lower with B[*a*]P exposure, but the difference was not statistically significant. Our results are in line with experiments with lymphocytes isolated from blood, which showed about 30% CD25 and 80% CD69 positive cells after stimulation with PMA and IO [22].

3.2. *Biotransformation of B[a]P*

In addition to B[*a*]P itself, trans-B[*a*]P-7,8-dihydrodiol, trans-B[*a*]P-9,10-dihydrodiol, B[*a*]P-tetrahydrotetrol, B[*a*]P-1,6-dione as well as 3-OH-B[*a*]P, 7-OH-B[*a*]P, 8-OH-B[*a*]P were measured to investigate the corresponding degradation pathways in Jurkat T cells. Intracellular B[*a*]P was detected in all samples. However, the only metabolite found was B[*a*]P-

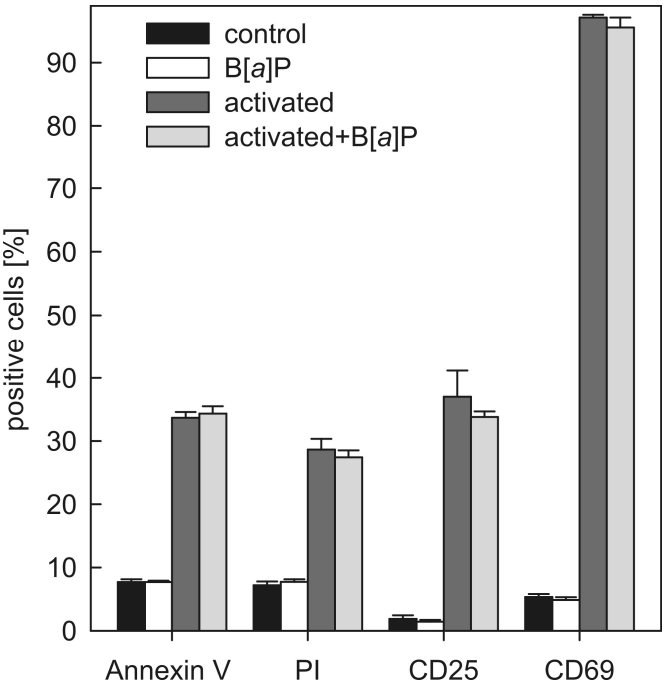

Figure 1. *Cell viability and activation status of Jurkat T cells after different treatments.* The viability and the activation status of the Jurkat T cells was analyzed by measurement of PI and annexin V staining as well as anti-CD25 or anti-CD69 staining via flow cytometry. Shown is the mean of three experiments ± SD.

1,6-dione (13.4 min). It was detected after exposure to 10 μM B[*a*]P for 4 h and 50 μM B[*a*]P for 4 h and 24 h (Figure S1) together with two other signals (13.7 min and 14.5 min) with the same MRM-transition (*m/z* 283->226). The data suggest that B[*a*]P is initially oxidized by P450 peroxidases or the monooxygenase catalytic cycle or by other peroxidases to form a B[*a*]P-cation. This reactive intermediate can either form DNA adducts or is metabolized further to B[*a*]P-1,6-dione.[8] The two unidentified peaks are likely to be other B[*a*]P-diones formed via the same metabolic pathway [23]. However, their further identification requires standard substances. For all other analyzed B[*a*]P-metabolites the concentrations were below the detection limit. Thus, it seems that in Jurkat cells B[*a*]P-dione formation via radical cation pathway is the main route of B[*a*]P-metabolism and –detoxification.

3.3. *Fractionation into different cellular compartments resulted in 2624 unambiguously identified proteins*

The proteome analysis yielded 2624 unambiguously identified proteins that were quantified by calculation of the peptide peak intensities (Table S1). With 1969 and 1842 hits, most of the proteins were found in the cytoplasm and membrane, respectively, whereas only 1506 proteins were identified in the nuclear fraction. In the cytoplasm and membrane fraction, similar numbers of proteins were quantified in all four different treatments, whereas in the nuclear fraction clearly more proteins (about 150 more) were quantified in the two activated samples. 1582 cytosolic, 970 nuclear and 1292 membrane proteins were used for enrichment and pathway analysis.

Based on the study of Beck *et al*. in 2011, which postulates a number of at least 10,000 proteins as typical for a human cell line [24], we achieved a reasonable coverage with a comparably simple fractionation method and only 108 LC-MS/MS runs. With the switch to a LC-MS/MS method we considerably improved the quantification rate compared to our previous B[*a*]P exposure experiments with Jurkat cells [14]. More precisely we identified and quantified in total 2624 proteins which is a 4-fold and 23-fold increase in comparison to the previously quantified and identified protein spots, respectively. The possibility of simultaneous identification and quantification of proteins by LC-MS is one of the clear advantages in comparison to gel-based approaches. Hence, the significance of subsequent pathway analysis is considerably improved.

In a global protein survey study on Jurkat T cells published in 2007, a total of 5381 proteins were identified with high confidence, but seven different cellular fractions, numerous replicates and about 16 times more LC-MS/MS runs than in our experiments had to be performed [25]. In respect to the nuclear fraction the number of 1506 detected proteins is higher than in another study that identified 872 proteins in the proteome of the T cell nucleolus [26]. De Wet *et al.* identified 1517 proteins in the T cell plasma membrane. In contrast, we were able to identify 325 additional proteins in the membrane fraction with more stringent identification criteria of at least two peptides and less LC-MS/MS runs as they cut every sample lane in ten pieces [27].

3.4. *Effects of activation and B[a]P on the proteome*

In order to understand the effect of activation on Jurkat T cells as well as the influence of B[*a*]P on this process, fold changes of the proteins as well as p-values were compared between the different treatments (Table S2). The significantly regulated proteins are visualized by plotting the log2 of the fold changes against the -log10 of the p-values (Figure 2A-D). B[*a*]P changes the expression of about 4% of the quantified proteins in the cytoplasm and membrane fraction (Figure 2E), whereas nearly no changes were detectable in the nuclear fraction (0.8%). Activation led to apparent changes of the protein abundance ranging from 5.3% to 16% in the three different cellular compartments in non-treated as well as in B[*a*]P exposed cells. Activation alone caused similar changes in the cytoplasm and nuclei fraction of about 12%, whereas activation in the presence of B[*a*]P modified the expression of nuclear proteins (16%) stronger than the expression of cytoplasmic proteins (9.2%). In addition, B[*a*]P exposure of activated cells caused only few significant changes in the proteome (0.9 - 1.4%) in all three fractions.

3.5. *Pathways influenced by activation and B[a]P exposure*

The abundance data from about 2500 proteins were analyzed using the Ingenuity Systems pathway program to unravel the affected cellular processes and pathways. The top ten regulated canonical pathways based on IPA p-values are summarized in Figure 3.

Effects of activation

Activation of Jurkat T cells affects the eIF2 pathway (Figure 3). Most of the quantified translation initiation factors and ribosomal proteins were down-regulated, and only very few were up-regulated. As the global regulation of translation mainly occurs by changes in the phosphorylation state of translation initiation factors [28], we analyzed the phosphorylation of eIF-2α (Figure 4A) and found that it was decreased in the activated cells. A reduced phosphorylation leads to an enhanced translation since the phosphorylation of eIF-2α inhibits the translation by blocking the GDP–GTP exchange on eIF2, which is required to reconstitute a functional complex for a new round of translation initiation [28]. This shows that changes in the protein abundance have to be carefully verified and that posttranslational modifications, especially phosphorylation, are very important for pathway regulation.

CD28 signaling in T helper cells is in the top ten of influenced pathways, which demonstrates on the proteomic level that the activation of the Jurkat cells was successful. Most of the proteins were found to be highly up-regulated, sometimes in several cellular fractions. NFKB1 and NFKB2 are induced by the CD28 co-stimulation pathway and play an important

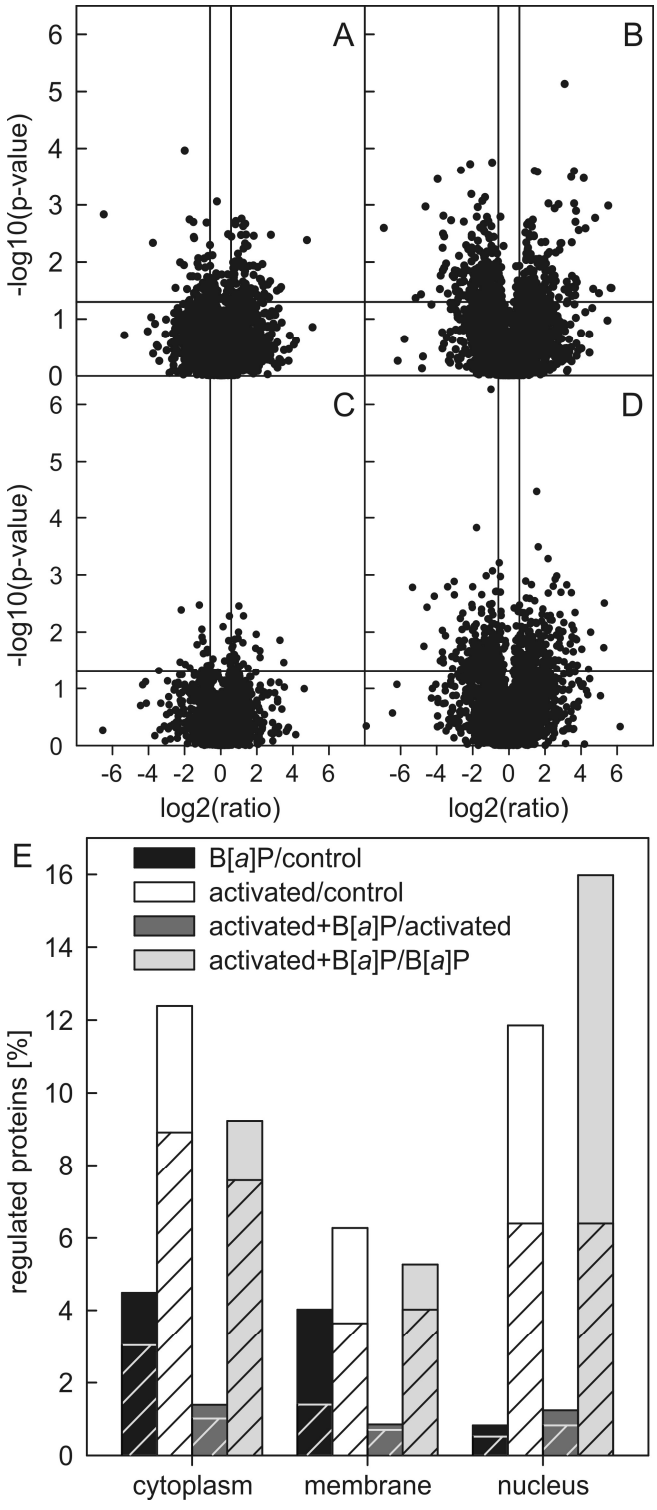

Figure 2. *Comparison of protein abundances between different treatments.* A-D: The log2 expression ratios are plotted against the -log10 of the p-values. The cutoffs for significantly changed proteins are indicated by solid lines (A - B[*a*]P/control; B - activated/control; C - activated+B[*a*]P/activated; D - activated+B[*a*]P/B[*a*]P); E: Shown is the distribution of differentially abundant proteins among the different compartments. Reduced protein abundance is illustrated by a fasciated pattern, increased protein abundance by no pattern.

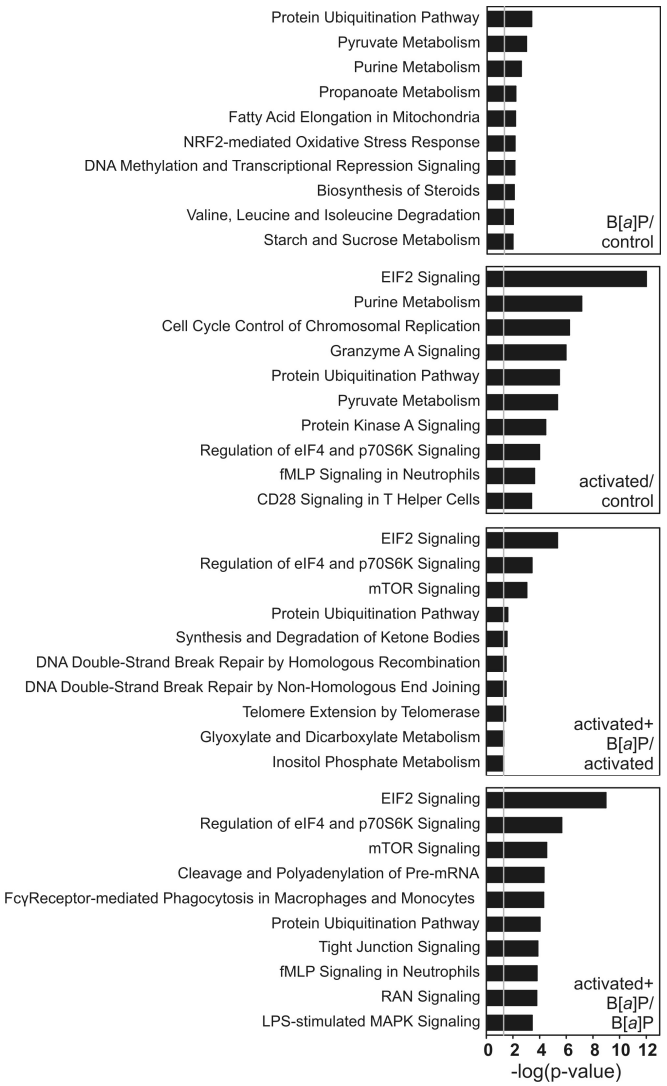

Figure 3. *Pathway analysis of proteins with Ingenuity IPA.* The bar chart displays the identified canonical pathways along with their significance (calculated by Ingenuity IPA). The top ten pathways are listed from most significant to least significant.

role in the regulation of the immune response, particularly for the transcription of cytokines such as IL-2 [29]. We verified the induced expression of NFKB1 by detecting its 120 kDa precursor as well as a substantial increase of the processed 50 kDa protein in the nucleus (Figure 4A). Furthermore, several actin-related proteins, α-actinin-1, vimentin and other proteins involved in reorganization of the cytoskeleton, were found to be significantly regulated. They are also important in T cell activation, especially in the formation of the immunological synapse [30].

Two metabolic pathways (purine and pyruvate metabolism) were identified and ranked within the top ten pathways by IPA. In order to confirm the results from pathway analysis we determined the concentrations of involved metabolites (Table S3). A significant down-regulation of AMP, ADP, ATP, UDP and UTP was observed and underlines the proteomic findings regarding nucleotide metabolism. In accordance

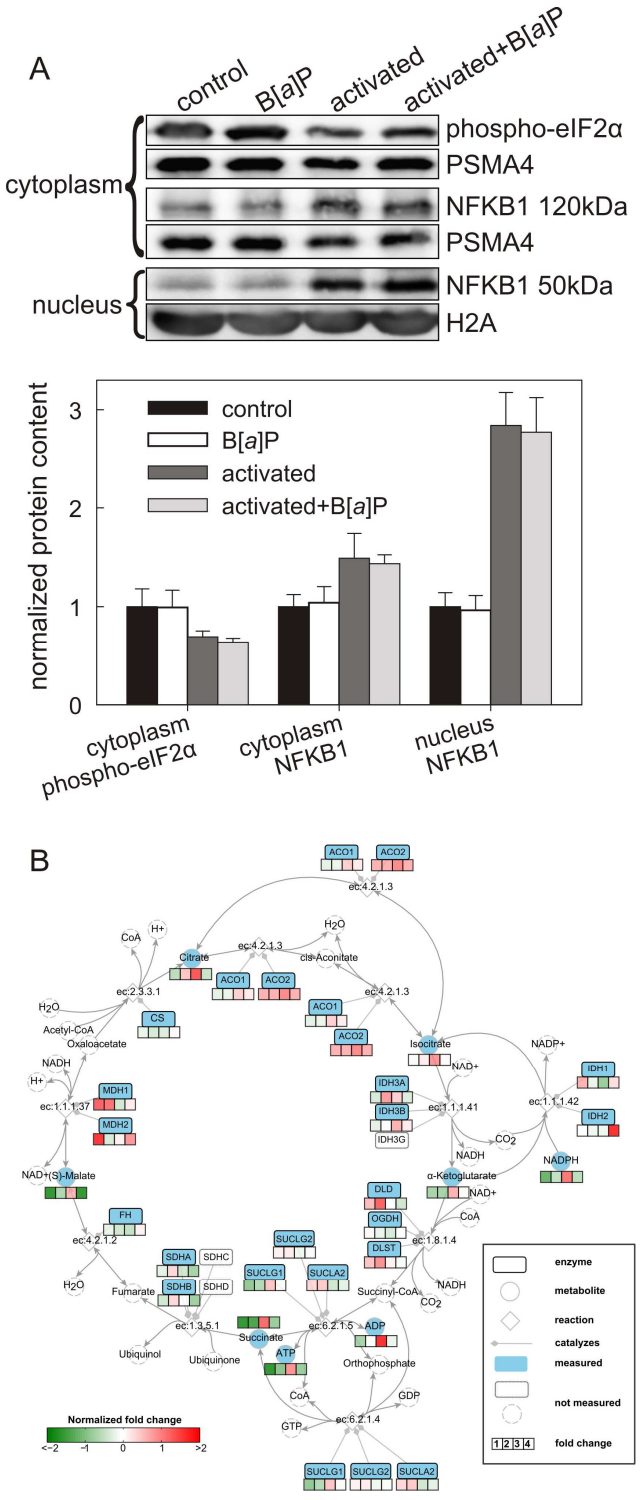

Figure 4. *Verification of proteomic results from LC-MS/M.* A: Shown are representative Western blots and the mean expression levels ± SD of NFKB1 and phospho-eIF2α from three replicates normalized to the indicated proteins used as input controls. B: Shown are the genes, metabolites and reactions involved in the citrate cycle. The normalized fold changes of the treatments are color -coded, which allows a comprehensible visualization of the integrated protein and metabolite data (1 - B[*a*]P/control; 2 - activated/control; 3 - activated+B[*a*]P/activated; 4 - activated+B[*a*]P/B[*a*]P).

to the influence of activation on the pyruvate metabolism, several enzymes and intermediates of the glycolysis such as hexokinase-1, phosphoenolpyruvate, glucose- and fructose 6-phosphate were up-regulated, although only pyruvate kinase isozymes M1/M2 and a subunit of the pyruvate dehydrogenase had a significantly increased expression. It is known that T cell stimulation leads to activation of the serine-threonine kinase AKT, which in turn promotes the localization of the glucose transporter GLUT1 to the membrane. This facilitates an increased glucose uptake, which was detected by a significant up-regulation of hexose concentration after activation [31]. Lactate and L-lactate dehydrogenase B chain were both significantly down-regulated, indicating that pyruvate may be metabolized in the citrate cycle rather than being dehydrogenated to lactate. Moreover, three intermediates of the citrate cycle, malate, succinate and α-ketoglutarate, were found to be down-regulated. Conversely, several citrate cycle enzymes were found to be induced, including the mitochondrial malate dehydrogenase. The opposite trends in regulation of enzymes and metabolites may be caused by the fact that the up-regulated enzymes efficiently metabolize their substrates and therefore their substrates are present in lower concentration, which is the case for malate and malate dehydrogenase. Glutamine, which was observed to be significantly up-regulated after T cell activation, can be deaminated in the mitochondria to generate α-ketoglutarate. This can be metabolized by the citrate cycle, regenerating the oxaloacetate required for continued biosynthesis. Even though glycolysis is regarded as the primary source of ATP generation in activated T cells, oxidative phosphorylation might represent an additional process for energy generation [32].

Effects of activation in the presence of B[a]P

According to IPA, the most striking effects of B[*a*]P on the activation process are changes in the pathway of cleavage and polyadenylation of pre-mRNA as well as in the mTOR and in the eIF4 and p70S6K signaling (Figure 3). The protein kinase mTOR acts as a central sensor and integrator of diverse environmental and metabolic influences. The best characterized downstream effectors of the mTOR signaling are the ribosomal protein p70S6K and eIF4EBP1. Both are phosphorylated in the activated mTOR pathway and promote translation initiation and therefore protein synthesis [33]. Furthermore, it is known that the mTOR signaling intersects with T cell metabolism and is involved in T cell fate decision and differentiation [6]. A disturbance in the mTOR pathway provoked by an environmental pollutant, such as B[*a*]P, could lead to an attenuation of the mTOR activity contributing to the down-regulation of T cell activity and even the induction of T cell anergy.

On the metabolic side we detected an increase of lysophosphatidylcholine concentrations after activation in the presence of B[*a*]P. Lysophosphatidylcholines play an important role in cell signaling via specific G-protein coupled receptors. It was shown that lysophosphatidylcholines activate the phos-

pholipase C, which releases diacylglycerols and IP_3, causing an increase in the intracellular Ca^{2+} concentration and the activation of the protein kinase C [34]. In addition, Okajima *et al.* demonstrated that the ability of IP_3 production in HL-60 leukemia cells depends on the fatty acid moieties of the phosphatidylcholines [35]. We detected significantly increased concentrations of 1-stearoyl lysophosphatidylcholine (lyso PC a C18:0) and additionally elevated levels of 1- lyso PC a C6:0, lyso PC a C14:0 and other lysophosphatidylcholines (fold changes 1.20 – 1.49).

In comparison to these results, the gel-based approach resulted in a more prominent identification of toxicological pathways such as AhR and NRF2 [14]. This is probably caused by the high abundance of proteins from these pathways (e.g. PRDX1, ACTB), which elevates the likeliness to detect them as affected proteins in gel-based approaches [36]. In contrast the effects on the mTor signaling and pre-mRNA processing found in this experiment depend as well on the quantification of less abundant proteins, again illustrating the value of LC-MS based approaches.

Effects of B[a]P exposure on non-activated cells

The B[*a*]P exposure of non-activated cells led to major changes in the cell metabolism as seven of the top ten pathways identified by Ingenuity are metabolic pathways (Figure 3). Several enzymes of the pyruvate, propanoate and fatty acid metabolism are up-regulated indicating a higher need for energy producing processes. Hexokinase-1, one of the key enzymes of glycolysis, which leads to pyruvate production, shows a 2.5-fold increased expression after B[*a*]P exposure. Hexokinases catalyze the ATP-dependent phosphorylation of glucose to yield glucose-6-phosphate and thereby control the first step of the glucose metabolism. Thus, they sustain the concentration gradient that permits facilitated glucose entry into cells and initiate all major pathways of glucose utilization [37]. In our previous work from Murugaiyan *et al.* we only identified the glutamine and pyrimidine metabolism as pathways affected by 50 nM B[*a*]P exposure in non-activated cells [14]. Hence, we obtained more detailed information about affected metabolic pathways in this new study.

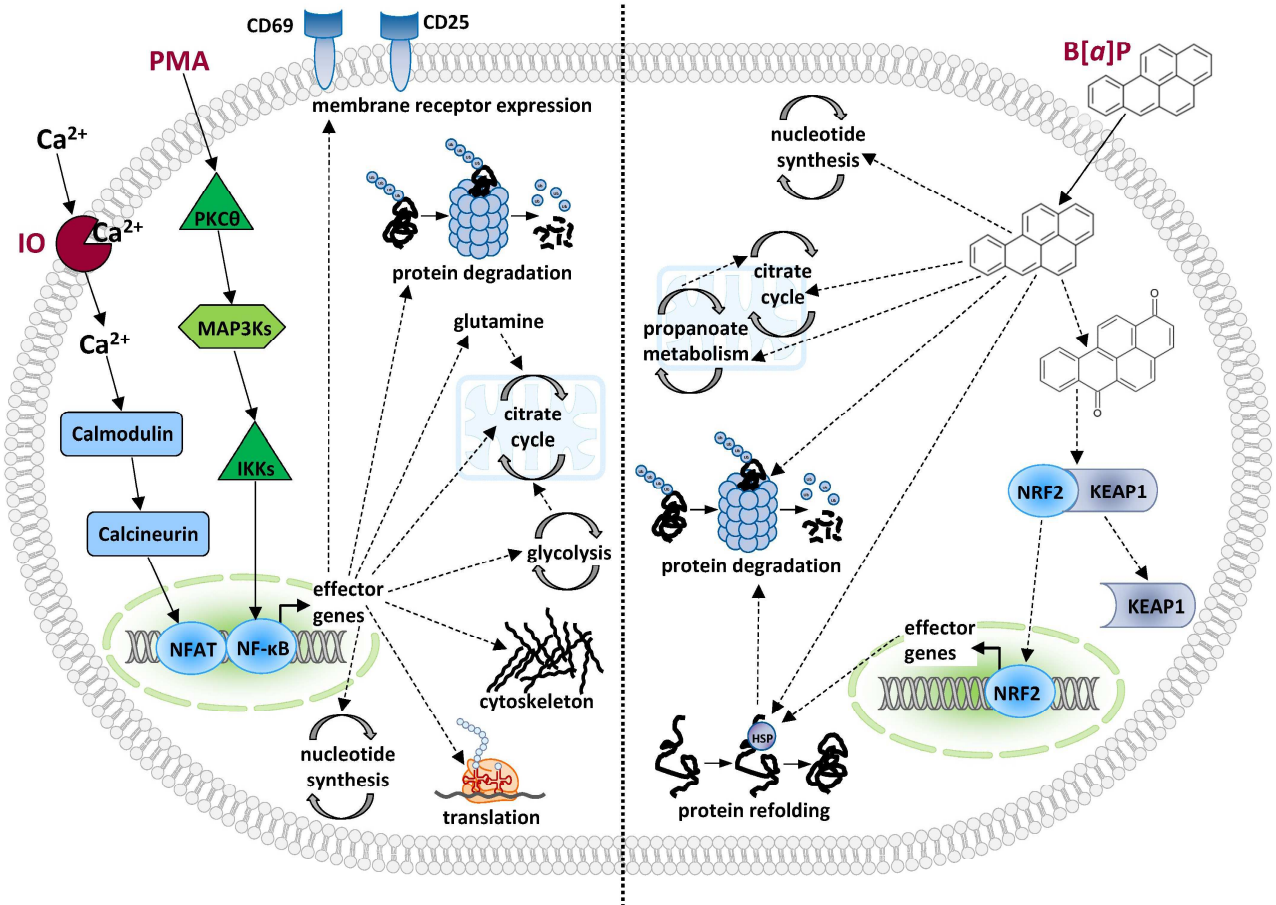

Figure 5. *Summary of signaling and metabolic pathways affected by activation and B[a]P exposure.* Shown is a summary of substances and intracellular pathways, which are affected by activation with PMA and IO (left side) or 50 nM B[*a*]P exposure (right side).

In order to further narrow down specifically affected areas in the metabolism, the integration of proteome and metabolome data was additionally performed by a random walks based approach. The enriched pathways and the corresponding biochemical connectivities between proteins and metabolites are shown in supplemental figure S2A-D. Since the citrate cycle was found to be affected under all examined treatments, it was chosen to illustrate the potential of integrated pathway analysis (Figure 4B). 22 different proteins covering nearly all reaction steps and the metabolites isocitrate, α-ketoglutarate, NADPH, ADP, ATP, succinate, malate and citrate as key molecules were detected. Three intermediates of the citrate cycle, malate, succinate and α-ketoglutarate, were found to be down-regulated. Conversely, several citrate cycle enzymes were found to be induced, including the mitochondrial malate dehydrogenase, indicating variations of enzyme activities rather than a simple abundance dependent correlation.

Our previous results indicated that B[*a*]P affects the IL-2 secretion as well as the glutamine and glutamate metabolism via the NRF2 pathway in Jurkat T cells [14]. Consistently, the NRF2 pathway is ranked on place six in this experiment, indicating a oxidative stress response after B[*a*]P exposure. Furthermore, we were able to show that B[*a*]P can be metabolized to B[*a*]P-quinones via the radical cation pathway. These quinones can undergo one-electron reduction by NAD(P)H-dependent reductases and form semiquinone anion radicals. The radicals redox-cycle back to diones in air and thereby generate ROS [9]. These reactive oxygen species can oxidize the disulfide bridges in KEAP1, which initiates the NRF2 pathway [38]. In addition to the transcriptional control of many phase I and phase II genes [12, 13] the NRF2 pathway can induce the expression of most proteasomal subunits [39] and heat shock proteins [40]. This connects it to the also identified ubiquitination pathway.

4. Concluding remarks

The effects of a subtoxic B[*a*]P concentration on activated and non-activated Jurkat T cells were revealed by proteomic and metabolomic profiling combined with pathway and network analysis. B[*a*]P is metabolized to B[*a*]P-1,6-dione and induces different metabolic pathways and the NRF2 pathway as a response to the electrophilic transformation products (Figure 5). Activation of Jurkat cells leads to pronounced changes, indicating strong adjustments in several metabolic pathways, protein and nucleotide synthesis (Figure 5). Although the effect of B[*a*]P is much stronger in non-activated cells, B[*a*]P seems to have an influence on the activation process suggesting an important role of the mTOR pathway in the cellular adaptation. The combined evaluation of proteome and metabolome data with an integrated, genome-scale metabolic model provided novel systems biological insights into the complex relation between metabolic and proteomic processes in Jurkat T cells during activation and subtoxic chemical exposure.

5. Supplementary material

Supplementary data and information is available at: http://www.jiomics.com/index.php/jio/rt/suppFiles/157/0

Supplemental Table 1 contains the protein identification and quantification data from MaxQuant.
Supplemental Table 2 shows the log-ratios and p-values of proteins for the four different comparisons. Only proteins identified in at least two of three replicates in all four treatments are listed.
Supplemental Table 3 shows the log-ratios and p-values of the quantified metabolites for the four different comparisons.
Supplemental Figure 1. MRM-chromatograms for the detection of B[*a*]P-1,6-dione using LCMS/MS.
Supplemental Figure 2. Metabolic subnetworks inferred from significantly changed proteins and metabolites by the kwalks approach.

Acknowledgments

This work was supported by the Helmholtz Impulse and Networking Fund through the Helmholtz Interdisciplinary Graduate School for Environmental Research (HIGRADE) and was funded in part by the European Research Council (starting grant 'LatentCauses'), by BMBF Grant no. 0315494A (project 'SysMBo') and by the DFG (SPP 'InKomBio'). The authors thank Silke Richter and Oliver Gericke for cooperation and technical assistance.

References

[1] D.D. Billadeau, J.C. Nolz, T.S. Gomez, Nat Rev Immunol, 7 (2007) 131-143. doi: 10.1038/nri2021

[2] R.T. Abraham, A. Weiss, Nat Rev Immunol, 4 (2004) 301-308. doi: 10.1038/nri1330

[3] E. Traxler, E. Bayer, J. Stockl, T. Mohr, C. Lenz, C. Gerner, Proteomics, 4 (2004) 1314-1323. doi: 10.1002/pmic.200300774

[4] M. Kobayashi, T. Katagiri, H. Kosako, N. Iida, S. Hattori, Electrophoresis, 28 (2007) 2035-2043. doi: 10.1002/elps.200600675

[5] V. Mayya, D.H. Lundgren, S.I. Hwang, K. Rezaul, L. Wu, J.K. Eng, V. Rodionov, D.K. Han, Sci Signal, 2 (2009) ra46. doi: 10.1126/scisignal.2000007

[6] K. Yang, H. Chi, Semin Immunol, 24 (2012) 421-428. doi: 10.1016/j.smim.2012.12.004

[7] P. Urso, N. Gengozian, R.M. Rossi, R.A. Johnson, J Immunopharmacol, 8 (1986) 223-241.

[8] D. Lu, R.G. Harvey, I.A. Blair, T.M. Penning, Chem Res Toxicol, 24 (2011) 1905-1914. doi: 10.1021/tx2002614

[9] H. Jiang, S.L. Gelhaus, D. Mangal, R.G. Harvey, I.A. Blair, T.M. Penning, Chem Res Toxicol, 20 (2007) 1331-1341. doi: 10.1021/tx700107z

[10] C. Esser, A. Rannug, B. Stockinger, Trends Immunol, 30 (2009) 447-454. doi: 10.1016/j.it.2009.06.005

[11] M. Veldhoen, J.H. Duarte, Curr Opin Immunol, 22 (2010) 747-752. doi: 10.1016/j.coi.2010.09.001

[12] M.E. Burczynski, T.M. Penning, Cancer Res, 60 (2000) 908-915.

[13] V.O. Tkachev, E.B. Menshchikova, N.K. Zenkov, Biochemistry (Mosc), 76 (2011) 407-422.

[14] J. Murugaiyan, M. Rockstroh, J. Wagner, S. Baumann, K. Schorsch, S. Trump, I. Lehmann, M. Bergen, J.M. Tomm, Toxicol Appl Pharmacol, 269 (2013) 307-316. doi: 10.1016/j.taap.2013.03.032

[15] F. Dautel, S. Kalkhof, S. Trump, J. Michaelson, A. Beyer, I. Lehmann, M. von Bergen, J Proteome Res, 10 (2011) 379-393. doi: 10.1021/pr100723d

[16] M. Rockstroh, S.A. Müller, C. Jende, A. Kerzhner, M. von Bergen, J.M. Tomm, JIOMICS, 1 (2011) 135-143.

[17] N. Morbt, J. Tomm, R. Feltens, I. Mogel, S. Kalkhof, K. Murugesan, H. Wirth, C. Vogt, H. Binder, I. Lehmann, M. von Bergen, J Proteome Res, 10 (2011) 363-378. doi: 10.1021/pr1005718

[18] A. Oberbach, M. Bluher, H. Wirth, H. Till, P. Kovacs, Y. Kullnick, N. Schlichting, J.M. Tomm, U. Rolle-Kampczyk, J. Murugaiyan, H. Binder, A. Dietrich, M. von Bergen, J Proteome Res, 10 (2011) 4769-4788. doi: 10.1021/pr2005555

[19] W. Röhmisch-Margl, C. Prehn, R. Bogumil, C. Röhring, K. Suhre, J. Adamski, Metabolomics, 8 (2011) 133-142.

[20] D.R. Green, N. Droin, M. Pinkoski, Immunol Rev, 193 (2003) 70-81.

[21] Y.J. Chwae, M.J. Chang, S.M. Park, H. Yoon, H.J. Park, S.J. Kim, J. Kim, J Immunol, 169 (2002) 3726-3735.

[22] M. Reddy, E. Eirikis, C. Davis, H.M. Davis, U. Prabhakar, J Immunol Methods, 293 (2004) 127-142. doi: 10.1016/j.jim.2004.07.006

[23] M. Huang, I.A. Blair, T.M. Penning, Chem Res Toxicol, 26 (2013) 685-692. doi: 10.1021/tx300476m

[24] M. Beck, A. Schmidt, J. Malmstroem, M. Claassen, A. Ori, A. Szymborska, F. Herzog, O. Rinner, J. Ellenberg, R. Aebersold, Mol Syst Biol, 7 (2011) 549. doi: 10.1038/msb.2011.82

[25] L. Wu, S.I. Hwang, K. Rezaul, L.J. Lu, V. Mayya, M. Gerstein, J.K. Eng, D.H. Lundgren, D.K. Han, Mol Cell Proteomics, 6 (2007) 1343-1353. doi: 10.1074/mcp.M700017-MCP200

[26] M.A. Jarboui, K. Wynne, G. Elia, W.W. Hall, V.W. Gautier, Mol Immunol, 49 (2011) 441-452. doi: 10.1016/j.molimm.2011.09.005

[27] B. de Wet, T. Zech, M. Salek, O. Acuto, T. Harder, J Biol Chem, 286 (2011) 4072-4080. doi: 10.1074/jbc.M110.165415

[28] F. Gebauer, M.W. Hentze, Nat Rev Mol Cell Biol, 5 (2004) 827-835. doi: 10.1038/nrm1488

[29] L. Tuosto, Immunol Lett, 135 (2011) 1-9. doi: 10.1016/j.imlet.2010.09.005

[30] J.K. Burkhardt, E. Carrizosa, M.H. Shaffer, Annu Rev Immunol, 26 (2008) 233-259. doi: 10.1146/annurev.immunol.26.021607.090347

[31] C. Mauro, H. Fu, F.M. Marelli-Berg, Curr Opin Pharmacol, 12 (2012) 452-457. doi: 10.1016/j.coph.2012.02.018

[32] R.G. Jones, C.B. Thompson, Immunity, 27 (2007) 173-178. doi:10.1016/j.immuni.2007.07.008

[33] B. Magnuson, B. Ekim, D.C. Fingar, Biochem J, 441 (2012) 1-21. doi: 10.1042/BJ20110892

[34] Y. Xu, Biochim Biophys Acta, 1582 (2002) 81-88.

[35] F. Okajima, K. Sato, H. Tomura, A. Kuwabara, H. Nochi, K. Tamoto, Y. Kondo, Y. Tokumitsu, M. Ui, Biochem J, 336 (Pt 2) (1998) 491-500.

[36] P. Wang, F.G. Bouwman, E.C. Mariman, Proteomics, 9 (2009) 2955-2966. doi: 10.1002/pmic.200800826

[37] R.B. Robey, N. Hay, Oncogene, 25 (2006) 4683-4696. doi: 10.1038/sj.onc.1209595

[38] P.M. Nguyen, M.S. Park, M. Chow, J.H. Chang, L. Wrischnik, W.K. Chan, Toxicol Sci, 116 (2010) 549-561. doi: 10.1093/toxsci/kfq150

[39] M.K. Kwak, N. Wakabayashi, J.L. Greenlaw, M. Yamamoto, T.W. Kensler, Mol Cell Biol, 23 (2003) 8786-8794.

[40] T. Rangasamy, C.Y. Cho, R.K. Thimmulappa, L. Zhen, S.S. Srisuma, T.W. Kensler, M. Yamamoto, I. Petrache, R.M. Tuder, S. Biswal, J Clin Invest, 114 (2004) 1248-1259. doi: 10.1172/JCI21146

JOURNAL OF INTEGRATED OMICS
A METHODOLOGICAL JOURNAL
HTTP://WWW.JIOMICS.COM

ORIGINAL ARTICLE | DOI: 10.5584/jiomics.v4i1.156

Molecular cloning and protein characterization of a heme-binding globin predicted in a sugar cane EST database

Daniel Henrique do Amaral Corrêa[1,#], Silvia Lucas Ferreira da Silva[1,#], Carlos Henrique Inácio Ramos [1,2,*]

[1]Institute of Chemistry, University of Campinas-UNICAMP, P.O. Box 6154, 13083-970 Campinas, SP, Brazil; [2]Instituto Nacional de Ciência e Tecnologia em Biologia Estrutural e Bioimagem, Brazil. [#] These authors contributed equally.

Received: 09 September 2013 **Accepted:** 29 December 2013 **Available Online**: 31 January 2014

ABSTRACT

A very large and representative sugar cane expression sequence tag (EST) library (SUCEST) was sequenced by a Brazilian consortium, opening the possibility to study important proteins, such as hemoglobins, which are largely present across the plant kingdom. The widespread presence and long evolutionary history of plant hemoglobins suggest a major role for this protein family in plants; however, little is known about their functional roles. In this study, we report the identification and characterization of a putative non-symbiotic hemoglobin cDNA clone that was identified in SUCEST. The cDNA was cloned, and the recombinant protein was purified and folded, as shown by its circular dichroism and emission fluorescence spectra. The expressed globin protein was able to bind hemin, as a characteristic Soret band was observed in the absorbance spectrum and increases were seen in the amount of secondary structure and in the stability of the protein. A model for the structure of the sugarcane hemoglobin was created using the crystal structure of a rice hemoglobin, and this model showed a conserved globular conformation.

Keywords: Sugar cane; Hemoglobin; Purification; Spectroscopy .

Abbreviations

Sc: Sugar cane; **Hb:** Hemoglobin; **EST:** expression sequence tag; **A:** absorbance; **CD:** circular dichroism; **PCR:** polymerase chain reaction; **SDS–PAGE:** sodium dodecyl sulfate-polyacrylamide gel electrophoresis.

1. Introduction

Globins are respiratory proteins that bind oxygen molecules through the iron ion of the porphyrin ring and a histidine in the polypeptide chain [1-3]. Globins are among the best-studied proteins when structure, function, and evolution are considered [1-3]. As a matter of fact, hemoglobin has been found in bacteria, plants, fungi, and animals. The first description of a plant hemoglobin was provided by Kubo [4], and since then, a large number of plant hemoglobins have been described [2,3,5]. Although hemoglobins were first identified in plant species that fix nitrogen via symbiosis with bacteria, it is likely that all plants have a hemoglobin gene, and in addition to the symbiotic leghemoglobins found in legumes, there may be another gene or gene family in legumes that encodes hemoglobins that function in non-symbiotic plant tissues [6]. In support of this notion, non-symbiotic hemoglobin genes were identified in both nitrogen - and non-nitrogen-fixing dicot species and in monocot species [2,3,5-8].

The widespread presence and long evolutionary history of plant hemoglobins suggest a major role for these proteins in plants [2], and thus, it is important to search for and characterize new proteins of this class to increase our general knowledge on this subject. Due to its major role in ethanol production, sugar cane has become of great importance in bioenergy studies, and to learn more about this plant, a Brazilian scientific consortium produced and sequenced a repre-

***Corresponding author:** Carlos Henrique Inácio Ramos, Institute of Chemistry, University of Campinas-UNICAMP, P.O. Box 6154, 13083-970 Campinas, SP, Brazil; E-mail address: cramos@iqm.unicamp.br, phone +55-19-3521-3096.

sentative expression sequence tag (EST) library from sugar cane (SUCEST) [9]. To gain information about hemoglobins in sugar cane, SUCEST was searched for a putative hemoglobin cDNA. Its cloning and protein purification and characterization are reported here. The recombinant protein was purified and folded, as shown by its circular dichroism and emission fluorescence spectra, and was able to bind hemin, as confirmed by the existence of a characteristic Soret band in the absorbance spectrum. This sugar cane hemoglobin showed an increase in secondary structure and stability when bound to heme, as is characteristic of globin family proteins. A structural model of the sugar cane hemoglobin was created using the crystal structure of a rice hemoglobin and showed a conserved globular conformation. These findings suggest that, like many plants, sugar cane expresses a heme-binding globin.

2. Material and Methods

2.1. *Cloning, expression and purification*

The cDNA library was constructed from a sugarcane cultivar that was a hybrid of crossing *Saccharum officinarum* with *Saccharum spontaneum* [9]. Blast searches of the database of expressed sequence tags SUCEST (http://sucest.lad.ic.unicamp.br/public) using the amino acid sequence of sperm whale myoglobin (GenBank accession number GI: 209563) as query revealed the sugar cane globin EST clone SCMCRZ3064B09.g (SUCEST). Sugar cane globin was amplified from the EST clone by PCR using primers 5´CAGTAGGTACATATGGGGTTC3´ and 5´CAGCCGGA TCCTTAGTCACGC3´ introducing *Nde*I and *Bam*HI restriction sites. The PCR product was digested and then inserted into the pET3a expression vector (Stratagene) to generate the pET3aScHb vector, which was confirmed by DNA sequencing. For protein expression, the construct was transformed into *Escherichia coli* BL21(DE3). The cells were grown in Luria Bertani medium at 37°C. When the A_{600} reached 0.8, 0.4 mM IPTG was added to induce protein expression [10] and the temperature was increased to 42°C for the production of inclusion bodies as previously described [11]. Four hours after expression was induced, the cells were harvested by centrifugation at 2,600 g and 4°C for 10 min, resuspended in 20 mL lysis buffer per L of culture, sonicated 12 times for 10 s each at 35 watts of output power with 2 min intervals and centrifuged at 13,000 g and 4°C for 10 min. The pellet, which contained the inclusion bodies, was washed 5 times with lysis buffer, resuspended in solubilization buffer by gentle agitation (60 min at room temperature) and centrifuged at 13,000 g and 4°C for 10 min. The supernatant, which contained the solubilized protein, was diluted twice with the same volume of equilibration buffer A and centrifuged as described above. The final supernatant was exhaustively dialyzed with equilibration buffer A. The sample was then loaded onto a Q Sepharose column (Pharmacia) equilibrated with 5 bed volumes of equilibration buffer A and recovered with increasing concentrations of NaCl (0 to 1 M). The fractions that contained the protein were pooled, exhaustively dialyzed with equilibration buffer B, loaded onto a HiLoad Superdex 200pg 26/60 molecular exclusion column (Pharmacia Biotech) equilibrated with 5 bed volumes of equilibration buffer B and recovered with the same buffer. Protein purification profiles were analyzed by SDS-PAGE as described by Laemmli [12]. The purified samples were exhaustively dialyzed in 20 mM Tris-HCl (pH 8.0), 1 mM EDTA, and 100 mM NaCl (buffer conditions for the experiments described below) and frozen for storage. The compositions of the working buffers were as follows. Lysis buffer: 100 mM Tris-HCl (pH 8.0), 100 mM KCl, 1 mM EDTA, 0.1 mM PMSF, 0.1 mM lysozyme, and 0.2% β-mercaptoethanol. Solubilization buffer: 100 mM Tris-HCl (pH 8.0) and 8 M GdnCl. Equilibration buffer A: 20 mM Tris-HCl (pH 8.0), 1 mM DTT and 1 mM EDTA. Equilibration buffer B: 20 mM Tris-HCl (pH 7.5), 1 mM DTT, 1 mM EDTA and 100 mM NaCl. The chemicals used were of analytical grade. All solutions were filtered, and their pH was checked before and after filtration.

2.2. *Concentration measurements and hemin binding*

The concentration of *Saccharum spp*. hemoglobin (ScHb) in the apo form was measured with a JASCO model 530 UV/VIS spectrometer using either the calculated extinction coefficient for denatured proteins [13,14] or the Bradford protein assay [15] using a commercial kit (Bio-Rad). For the preparation of the protein in the holo form, hemin was mixed with the protein solution at a 1:2 ratio (protein:hemin) and incubated at 4°C for 30 min, followed by centrifugation at 90,000 g and 4°C for 20 min to eliminate any of the remaining apo form, as previously described for recombinant sperm whale myoglobin [11]. The concentration of holoScHb was measured at the Soret band in 20 mM sodium phosphate (pH 7.0), as described by Antonini and Brunori [16].

2.3. *Spectroscopic experiments*

A JASCO model J-810 Circular Dichroism (CD) spectropolarimeter equipped with a thermoelectric sample temperature controller (Peltier system) was used to record the CD spectra. The data were collected from 260 nm to 200 nm and accumulated at least 16 times for the spectral measurements. The data were collected at 222 nm for the stability measurements, and each plotted CD signal at 222 nm was the average of 5-min recordings. The CD measurements were made in cuvettes with a 1-mm path length at 20°C, and the thermal-induced unfolding and refolding was recorded every 1°C at a scan rate of 60°C/h. The average of at least three unfolding experiments was used to build each curve profile. The fluorescence measurements were collected using an Aminco Bowman Series 2 luminescence spectrometer (SLM Aminco) and a 1 x 1-cm path length cuvette with 2 μM apoScHb at 20°C. Excitation was at 280 nm with a bandpass of 2 nm, and emission was measured from 300 to 400 nm with a bandpass of 8

nm. The intrinsic emission fluorescence data were analyzed by either their emission maxima wavelength or their spectral center of mass (<λ>), as described by the equation below:

$$<\lambda> = \sum\lambda_i F_i / \sum F_i \qquad \text{[Equation 1]}$$

where λ_i is each wavelength and F_i is the fluorescence intensity at λ_I [17]. Curve fitting was accomplished with Origin (Microcal Software). Unless stated otherwise, the experimental error was less than 5%.

2.4. *Structural modelling*

The structure of *Oryza sativa* non-symbiotic hemoglobin 1 (PDB 1D8U chain A), which shares 66% sequence identity with ScHb (Table 1), was used as a template to model the structure of ScHb. First, the HHpred server (toolkit.tuebingen.mpg.de/hhpred) [18] was used to generate a homology model for ScHb, and then, the stereochemical quality of the model was assessed using the PROCHECK server (swissmodel.expasy.org/workspace/index.php?func=tools_structureassessment1) [19].

3. Results and Discussion

3.1. *Sugar cane hemoglobin*

Proteins are important biomolecules that are involved in the majority of the physiological functions of a cell. Thus, to learn how a cell functions, information can be gathered about the proteins that are expressed during the life of the cell and how these proteins are chemically modified. This large amount of information is called the cell proteome and requires tremendous effort to complete. Proteins are produced by the ribosomal machinery from the information encoded in mRNAs, and thus, even the information in the mRNA alone is important to gain information about the cell proteome. As a consequence, expressed sequence tag (EST) projects have been used as low-cost alternatives to complement genome and proteome projects [20]. An EST project for sugar cane was completed by a Brazilian scientific consortium (SUCEST), and the resulting database is currently available [9]. We searched this database for a putative heme-binding globin and identified a candidate (Fig. 1) that has high identity with heme-binding globins from several organisms (Table 1). To further characterize this gene as a hemoglobin, we cloned the cDNA, purified the recombinant protein, characterized its folded state and tested whether the globin was able to bind heme.

Fig. 1 shows the nucleotide sequence and the deduced amino acid sequence of the sugar cane hemoglobin (ScHb). The amino acid sequence of ScHb was submitted to Pfam (http://pfam.sanger.ac.uk/), a database with a large collection of protein families, which found a significant (e-value of 8.8e-21) globin domain match starting at residue 7 and ending at residue 118. ScHb was 188 residues long and had a high identity (approximately 83%) with a hemoglobin from *Zea mays*, which is 191 residues long (Table 1). ScHb is more closely related to *Arabidopsis* AHb1 (GLb1) than AHb2 (GLb1). AHb1 has a sequence and oxygen-binding characteristics that are typical of stress-induced hemoglobins, and its overexpression protects *Arabidopsis thaliana* from the effects of severe hypoxia [21], whereas AHb2 has greater similarity to symbiotic hemoglobins in both its sequence and oxygen-binding characteristics [22]. Whether ScHb functions in the stress response requires further investigation. However, because most genes with high identity to ScHb were classified as non-symbiotic hemoglobin class 1 (Table 1), we suggest that the sugar cane gene investigated here also belongs to this class.

Table 1. Amino acid sequence homology between sugar cane hemoglobin and other globins.

Protein identification	Gen bank accession number	Organism	Number of residues	Identity (%)
hemoglobin	GI:74058375	*Zea mays*	191	83
unknown protein with globin domain	GI:50932383	*Oryza sativa*	145	79
non-symbiotic hemoglobin class 1	GI:17366135	*Oryza sativa*	166	66
non-symbiotic hemoglobin class 1	GI:15809394	*Citrus unshiu*	183	65
hemoglobin	GI:2071976	*Hordeum vulgare*	162	63
hemoglobin Hb1	GI:27085255	*Triticum aestivum*	162	63
non-symbiotic hemoglobin 1 GLB1	GI17432970	*Arabidopsis thaliana*	160	63
non-symbiotic hemoglobin 2 GLB2	GI:17432971	*Arabidopsis thaliana*	158	54
myoglobin	GI:209563	*Physeter catodon*	153	20

ATG	GGG	TTC	AGT	GAG	GCA	CAG	GAA	GAG	CTT	GTC	ATC	CGT	TCA
M	G	F	S	E	A	Q	E	E	L	V	I	R	S
TGG	AAA	GCC	ATG	AAG	AAC	GAC	TCC	GAG	TCA	ATC	GCT	CTT	AAG
W	K	A	M	K	N	D	S	E	S	I	A	L	K
TTC	TTC	CTC	AGG	ATC	TTT	GAG	ATC	GCG	CCG	GAT	GCC	AAG	CAG
F	F	L	R	I	F	E	I	A	P	D	A	K	Q
ATG	TTC	TCC	TTC	CTG	CGC	GAC	GAC	GCC	GGC	GAC	GCG	ACC	CTG
M	F	S	F	L	R	D	D	A	G	D	A	T	L
GAG	AAC	CAC	CCC	AAG	CTC	AAG	GCG	CAC	GCC	GTC	ACC	GTC	TTC
E	N	H	P	K	L	K	A	H	A	V	T	V	F
GTC	ATG	GCT	TGC	GAG	TCC	GCG	ACG	CAG	CTG	AGG	AGC	ACC	GGC
V	M	A	C	E	S	A	T	Q	L	R	S	T	G
GAC	GTG	AAG	GTG	AGG	GAG	GCC	ACC	CTG	AAG	CGG	CTG	GGC	GCG
D	V	K	V	R	E	A	T	L	K	R	L	G	A
ACG	CAC	GTC	AAG	GCG	GGC	GTC	GCC	GAC	GCG	CAT	TTC	GAG	GTC
T	H	V	K	A	G	V	A	D	A	H	F	E	V
GTA	AAG	ACG	GCG	CTG	CTG	GAC	ACC	ATC	AGG	GAC	GCG	GTC	CCG
V	K	T	A	L	L	D	T	I	R	D	A	V	P
GAC	AGG	TGG	ACG	CCG	GAA	ATG	AAG	GCG	GCG	TGG	GAG	GAG	GCC
D	R	**W**	T	P	E	M	K	A	A	**W**	E	E	A
TAC	GAC	CAG	CTG	GCC	GCC	GCC	ATC	AAG	GAG	GAG	ATG	AAG	AAC
Y	D	Q	L	A	A	A	I	K	E	E	M	K	N
GGC	GCC	GTC	AAG	GAG	GAG	ATG	AAG	AAC	GGC	GCC	GTC	AAG	GAG
G	A	V	K	E	E	M	K	N	G	A	V	K	E
GAG	ACG	AAG	GAC	GCC	GCC	GCG	GCT	CGA	TGG	TTC	CTA	TGC	TCC
E	T	K	D	A	A	A	A	R	**W**	F	L	C	S
TCC	GCT	AGC	TCG	CGT	GAC	TAA							
S	A	S	S	R	D	**STOP**							

Figure 1. DNA nucleotide sequence and deduced amino acid sequence of the sugar cane hemoglobin gene. Nucleotides and amino acid residues are represented by an one-letter code. The initial ATG codon and the STOP codon are in bold, and the Trp residues (W) are in red.

As a matter of fact, non-symbiotic hemoglobin genes have already been identified in several plants [5-8].

3.2. *Protein production*

Protein expression was induced at 42°C to induce the formation of inclusion bodies, from which it is possible, after a few steps, to purify a folded globin protein in the apo form, as previously reported [11]. Under this expression condition, apoScHb was the major protein present in the inclusion body fraction and was solubilized by the addition of a chemical denaturant. Thereafter, it was dialyzed and then loaded onto a Q Sepharose column (Fig. 2, lane 1) and purified (Fig. 2, lane 2). The fraction from the last step, which contained apoScHb, was dialyzed and then loaded onto a High Load Superdex 200pg 26/60 column for the final chromatographic step (Fig. 2, lane 3). The final protein product was pure, with a yield of approximately 24 mg/mL (Table 2).

The folded state of apoScHb was first investigated by fluorescence. The fluorescence of Trp is very sensitive to the polarity of the environment, thus allowing insight on whether the residue is buried in the apolar interior of the protein or exposed to the solvent. ScHb has four Trp residues (Fig. 1), and its emission fluorescence spectroscopy spectrum is shown in Fig. 3A. The emission fluorescence spectrum has a maximum intensity at 337 nm with center of mass of 342 nm (Table 2), indicating that the Trp residues were well buried in the globin protein. This result was characteristic of a well-folded protein in which the hydrophobic Trp residues are buried and the hydrophilic residues are at the surface. Because the observed fluorescence spectrum is the sum of each Trp fluorescence spectrum, only an average evaluation of the Trp environment is possible. However, further indication of our purified apoScHb as a well-folded protein was also provided by circular dichroism (CD) studies (Fig. 3B). Circular dichroism is a fast and reliable tool to evaluate the secondary structure of a protein and, thus, its folded state [23]. The far-UV spectrum of apoScHb was characteristic of an α-helical protein with minima at 208 and 222 nm (Fig. 3B), and the secondary structural prediction indicated that it was approximately 68% α-helical (Table 2). These results are in good agreement with a globin fold, in which a large α-helical content is characteristic even for the apo form of the protein [24].

3.3. *Heme binding*

Because the cDNA annotated as a hemoglobin encoded a protein with a fold that is characteristic of the globin family, we tested whether this protein is able to bind heme and if this binding caused conformational changes in the protein. Hemin binding was evaluated as previously described for recombinant sperm whale myoglobin [11] using the absorbance spectra of apo and holoScHb from 250 to 600 nm (Fig. 3C). ApoScHb showed absorption at approximately 280 nm due to its aromatic residues and showed no significant absorption in the visible region (Fig. 3C, Table 2), whereas holoScHb also showed absorption at approximately 280 nm due to its aromatic residues and had an absorption peak at 416 nm, the Soret absorption peak of bound hemin (Fig. 3C,

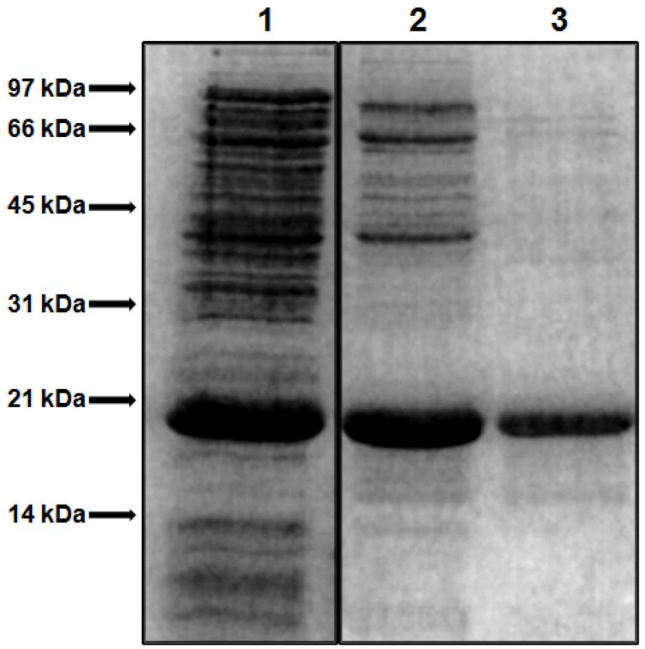

Figure 2. SDS-PAGE showing the ScHb purification steps (see Material and Methods). Lane 1, Sample prior to loading onto a Q Sepharose column. Lane 2, pool of ScHb purified from the Q Sepharose column. Lane 3, pool of ScHb purified from the High Load Superdex 200pg 26/60 column. The resulting ApoScHb was pure, with a yield of approximately 24 mg/mL (Table 2). The molecular mass standards are shown on the right (arrows).

Table 2. ScHb parameters.

	Apo ScHb	Holo ScHb
Yield (mg/L)	24	-
Emission fluorescence maximum wavelength (nm)	337	-
Emission fluorescence spectral center of mass (nm)	342	-
A_{416}/A_{280}	0.06	2.63
α-helical content (%)	68	87

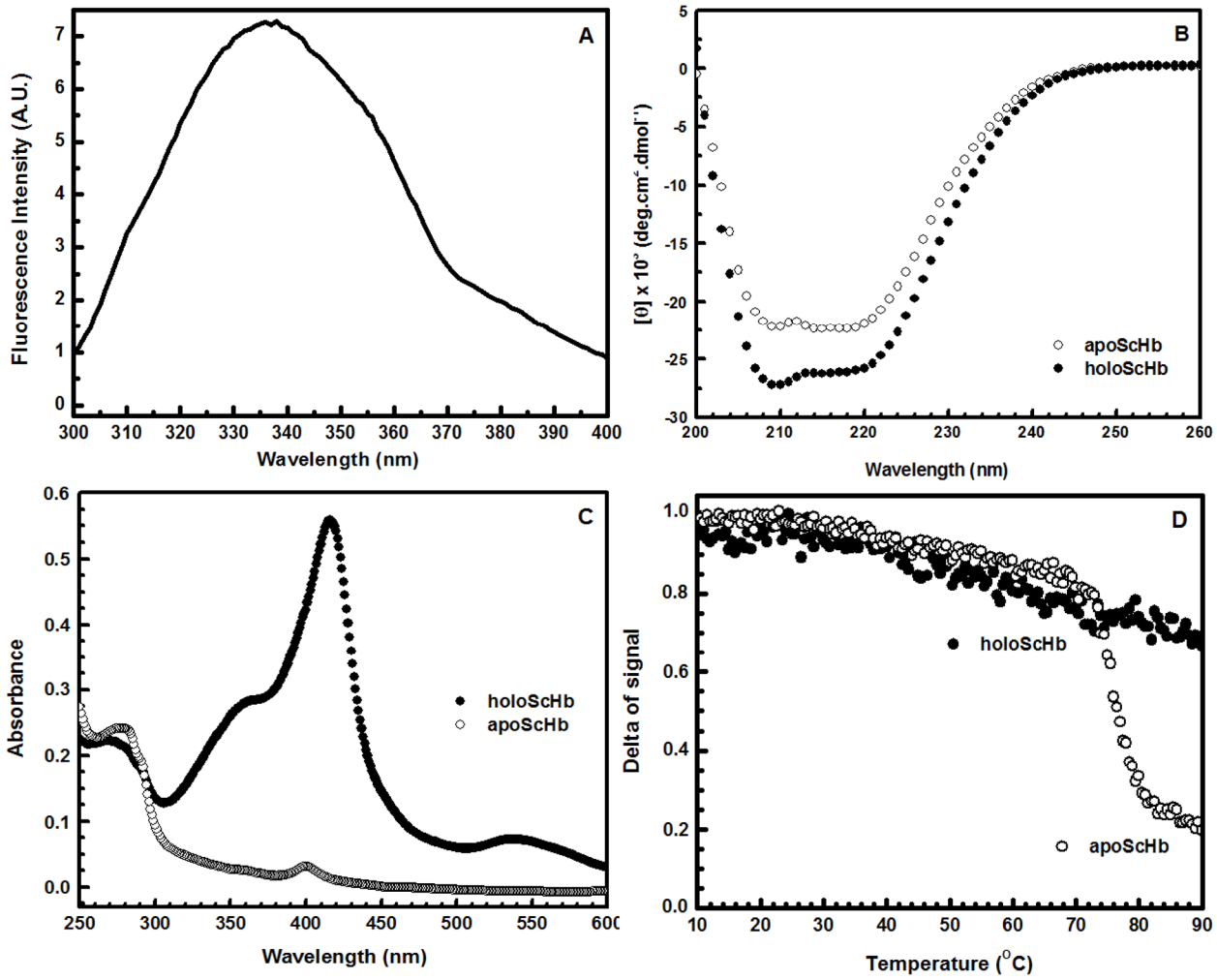

Figure 3. Spectroscopic experiments. A) Fluorescence. The emission fluorescence spectrum was measured from 300 to 400 nm and had a maximum intensity at 337 nm with a center of mass of 342 nm. B) Circular dichroism. The circular dichroism (CD) spectra of apoScHb (open circles) and holoScHb (filled circles) were measured from 200 to 260 nm. The CD spectra of both forms showed minima at 208 and 222 nm, a characteristic of α-helical proteins. C) Absorbance. The absorbance of untreated (apo, open circles) and treated (holo, filled circles) ScHbs were measured in the UV and Soret regions (250-600 nm). Peaks at 280 nm, due to aromatic residues, and at 540 and 416 nm, which are indicative of native-like heme coordination, were present in the spectrum of holoScHb. D) Thermal-induced unfolding followed by CD. Thermal-induced unfolding was monitored by CD at 222 nm from 10 to 90°C. ApoScHb (open circles) had an unfolding transition starting at approximately 72°C with a midpoint at approximately 75°C, while holoScHb (filled circles) showed no apparent transition even at 90°C.

Table 2). Another absorption peak at 540 nm was present in the holoScHb spectrum (Fig. 3C), which is also considered to be characteristic of specific heme binding [25]. These absorption peaks are not caused by free hemin because the spectrum of free hemin is characterized by two large maxima of the same magnitude at approximately 340 and 400 nm and by a small minimum at approximately 600 nm (data not shown). Additionally, holoScHb had typical characteristics of hologlobins. HoloScHb had both a higher amount of secondary structure than the apo form (87% and 68%, respectively) (Fig. 3B and Table 2) and a higher stability, as shown by thermal-induced unfolding experiments (Fig. 3D). Thermal-induced unfolding was monitored by CD at 222 nm. ApoScHb had an unfolding transition starting at approximately 72°C, with a midpoint at approximately 75°C, while holoScHb showed no apparent transition even at 90°C (Fig. 3D). Increases in both secondary structure and stability as a consequence of heme binding have been reported for several globin proteins [26-29].

The above results provide strong support to the hypothesis that the gene predicted as a hemoglobin in the sugar cane EST database does indeed code for a protein with a globin fold. Therefore, the three-dimensional structure of ScHb is likely to be similar to that of other hemoglobins because globins are strikingly similar to each other despite extensive variations in amino acid sequence. Additionally, the array of α-helices that constitutes the globin protein fold has been conserved throughout the evolution of plants and animals [30]. The structure of the *Oryza sativa* non-symbiotic hemoglobin GLB1a (PDB 1D8U chain A; Fig. 4, top A), which shares 66% sequence identity with sugar cane Hb (Table 1 and Fig. 4, bottom), was used as a template to model the structure of ScHb (Fig. 4, top B). The final model of ScHb had good stereochemical quality according to the Ramchandran plot (Supplementary Fig. 1). The residues in most favored regions, residues in additional allowed regions, residues in generously allowed regions, and residues in disallowed regions were 89.4%, 7.0%, 2.8%, and 0.7%, respectively (Supplementary Fig. 1), confirming the geometrically acceptable quality of the model. The globular fold of the ScHb model and the relative position of the α-helices were very similar to those of GLB1a (Fig. 4). The Sc hemoglobin length of 188 amino acids exceeds the lengths of vertebrate myo- and hemoglobins and results from a C-terminal protein extension, whose functional relevance is unclear. However, the globin fold was conserved, as shown in Fig. 4 (top B), and the proximal and distal histidines in positions E7 and F8 as well as the phenylalanine at the CD1 corner were present in ScHb (Fig. 4, top B). Thus, the key residues that are important for the function of ScHb as a typical oxygen binding protein are strictly conserved. The class 1 and 2 Hbs [31] of plants are similar to vertebrate Hbs in that all of these molecules have an E7 histidine residue, which is necessary for binding oxygen and other ligands in the distal pocket of the molecule. Altogether, these results also support the hypothesis that the protein studied here is indeed a hemoglobin.

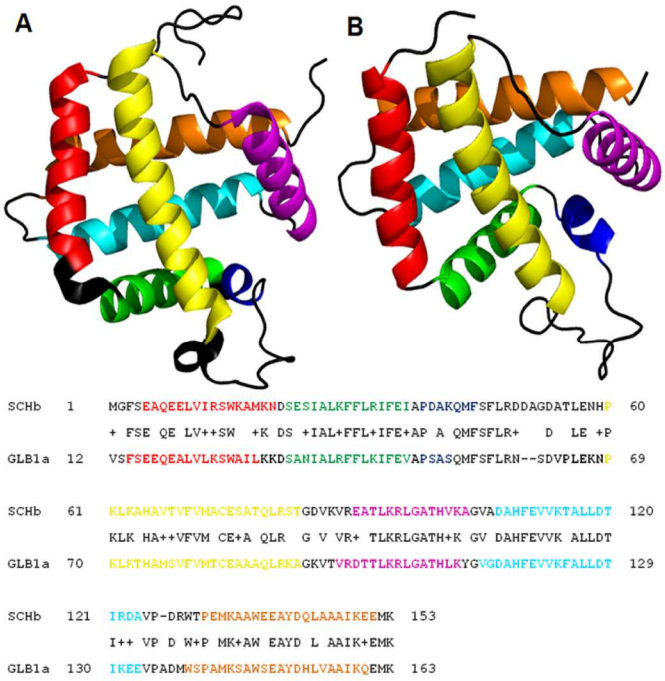

Figure 4. The structure of ORYsa GLB1a (PDB: 1D8U, top A) was used as a template to model the structure of ScHb (top B) by homology. The HHpred server [18] was used to generate a homology model for the *Saccharum officinarum* globin protein ScHb. The images were produced using PyMol (PyMOL Molecular Graphics System, Version 1.3, Schrödinger, LLC). The amino acid alignment is shown at the bottom (only amino acids 1-153 of ScHb are shown), and colors were used to label the α-helices in both the amino acid sequence and the structures.

4. Concluding Remarks

We report the identification of a heme-binding globin in sugar cane. A gene coding for hemoglobin in sugarcane was predicted from an EST database [9] and mRNA expression data [32]. Sugar cane hemoglobin was purified as a soluble protein and in its apo form, i.e., without heme bound. The apoprotein was able to bind heme, as seen by the existence of a characteristic Soret band and an increase in secondary structure, as is expected for its holo form. The widespread presence and long evolutionary history of plant hemoglobins suggest a major role for these proteins in plants; however, little is known about their function. The identification of this gene in sugar cane supports the hypothesis that non-symbiotic hemoglobin genes are present in all plants.

5. Supplementary Material

Supplementary data and information is available at: http://www.jiomics.com/index.php/jio/rt/suppFiles/156/0

Supplemental Figure 1. Ramachandran plot of the ScHb 3D model, which was based on the structure of ORYsa GLB1a (PDB: 1D8U-A). The plot shows the acceptability of the model.

Acknowledgements

The authors thank Fundação de Amparo à Pesquisa do Estado de São Paulo (FAPESP), and Ministério da Ciência e Tecnologia/Conselho Nacional de Desenvolvimento Científico e Tecnológico (MCT/CNPq) for financial support and fellowships.

References

[1] R.E. Dickerson, I. Geis, Hemoglobin: structure, function, evolution, and pathology, Benjamin/Cummings Pub. Co., 1983.

[2] J.A. Hoy, M.S. Hargrove, Plant Physiol Biochem, 46 (2008) 371-379. doi: 10.1016/j.plaphy.2007.12.016

[3] K.J. Gupta, K.H. Hebelstrup, L.A. Mur, A.U. Igamberdiev, FEBS Lett, 585 (2011) 3843-3849. doi: 10.1016/j.febslet.2011.10.036

[4] H. Kubo, Acta Phytochim., 11 (1939) 195-200.

[5] C. Dordas, J. Rivoal, R.D. Hill, Ann Bot, 91 Spec No (2003) 173-178. doi: 10.1093/aob/mcf115

[6] D. Bogusz, C.A. Appleby, J. Landsmann, E.S. Dennis, M.J. Trinick, W.J. Peacock, Nature, 331 (1988) 178-180. doi: 10.1038/331178a0

[7] E.R. Taylor, X.Z. Nie, A.W. Macgregor, R.D. Hill, Plant Molecular Biology, 24 (1994) 853-862. doi: Doi 10.1007/Bf00014440

[8] B. Trevaskis, R.A. Watts, C.R. Andersson, D.J. Llewellyn, M.S. Hargrove, J.S. Olson, E.S. Dennis, W.J. Peacock, Proc Natl Acad Sci U S A, 94 (1997) 12230-12234. doi: 10.1073/pnas.94.22.12230

[9] A.L. Vettore, F.R. da Silva, E.L. Kemper, P. Arruda, Genetics and Molecular Biology, 24 (2001) 1-7. doi: 10.1590/s1415-47572001000100002

[10] F. William Studier, A.H. Rosenberg, J.J. Dunn, J.W. Dubendorff, 185 (1990) 60-89. doi: 10.1016/0076-6879(90)85008-c

[11] E.A. Ribeiro, Jr., W.C. Regis, L. Tasic, C.H. Ramos, Protein Expr Purif, 28 (2003) 202-208. doi: 10.1016/s1046-5928(02)00651-4

[12] U.K. Laemmli, Nature, 227 (1970) 680-685. doi: 10.1038/227680a0

[13] H. Edelhoch, Biochemistry, 6 (1967) 1948-1954. doi: 10.1021/bi00859a010

[14] S.C. Gill, P.H. von Hippel, Anal Biochem, 182 (1989) 319-326. doi: 10.1016/0003-2697(89)90602-7

[15] M.M. Bradford, Anal Biochem, 72 (1976) 248-254. doi: 10.1016/0003-2697(76)90527-3

[16] E. Antonini, M. Brunori, eds., Hemoglobin and Myoglobin in their Reactions with Ligands, American Elsevier, New York, 1971.

[17] J.L. Silva, E.W. Miles, G. Weber, Biochemistry, 25 (1986) 5780-5786. doi: 10.1021/bi00367a065

[18] J. Soding, A. Biegert, A.N. Lupas, Nucleic Acids Res, 33 (2005) W244-248. doi: 10.1093/nar/gki408

[19] R.A. Laskowski, J.A. Rullmannn, M.W. MacArthur, R. Kaptein, J.M. Thornton, J Biomol NMR, 8 (1996) 477-486. doi: 10.1007/bf00228148

[20] J. Parkinson, M. Blaxter, Methods Mol Biol, 533 (2009) 1-12. doi: 10.1007/978-1-60327-136-3_1

[21] P.W. Hunt, E.J. Klok, B. Trevaskis, R.A. Watts, M.H. Ellis, W.J. Peacock, E.S. Dennis, Proc Natl Acad Sci U S A, 99 (2002) 17197-17202. doi: 10.1073/pnas.212648799

[22] R. Arredondo-Peter, M.S. Hargrove, J.F. Moran, G. Sarath, R.V. Klucas, Plant Physiol, 118 (1998) 1121-1125. doi: 10.1104/pp.118.4.1121

[23] D.H.A. Corrêa, C.H.I. Ramos, Afr J Biochem Res 3(2009) 9.

[24] W.C. Regis, J. Fattori, M.M. Santoro, M. Jamin, C.H. Ramos, Arch Biochem Biophys, 436 (2005) 168-177. doi: 10.1016/j.abb.2005.01.016

[25] C.S. Craik, S.R. Buchman, S. Beychok, Proc Natl Acad Sci U S A, 77 (1980) 1384-1388. doi: 10.1073/pnas.77.3.1384

[26] E. Breslow, S. Beychok, K.D. Hardman, F.R. Gurd, J Biol Chem, 240 (1965) 304-309.

[27] Y.Q. Feng, S.G. Sligar, Biochemistry, 30 (1991) 10150-10155. doi: 10.1021/bi00106a011

[28] C.H. Ramos, M.S. Kay, R.L. Baldwin, Biochemistry, 38 (1999) 9783-9790. doi: 10.1021/bi9828627

[29] D.A. Landfried, D.A. Vuletich, M.P. Pond, J.T. Lecomte, Gene, 398 (2007) 12-28. doi: 10.1016/j.gene.2007.02.046

[30] D. Bashford, C. Chothia, A.M. Lesk, J Mol Biol, 196 (1987) 199-216. doi: 10.1016/0022-2836(87)90521-3

[31] P.W. Hunt, R.A. Watts, B. Trevaskis, D.J. Llewelyn, J. Burnell, E.S. Dennis, W.J. Peacock, Plant Molecular Biology, 47 (2001) 677-692. doi: 10.1023/a:1012440926982

[32] R. Linacero, M.G. Lopez-Bilbao, A.M. Vazquez, Protoplasma, 217 (2001) 199-204. doi: 10.1007/BF01283401

JOURNAL OF INTEGRATED OMICS
A METHODOLOGICAL JOURNAL
HTTP://WWW.JIOMICS.COM

ORIGINAL ARTICLE | DOI: 10.5584/jiomics.v4i1.168

2D DIGE proteomic analysis of multidrug resistant and susceptible clinical *Mycobacterium tuberculosis* isolates

Truong Quoc Phong*[1], Elke Hammer[2], Manuela Gesell Salazar[2], Do Thi Thu Ha[1], Nguyen Lan Huong[1], Dang Minh Hieu[1], Nguyen Thanh Hoa[1], Phung Thi Thuy[1], Uwe Volker[2]

[1] Center for Research and Development in Biotechnology, Hanoi University of Science and Technology, Vietnam; [2] Interfaculty Institute for Genetic and Functional Genomic, Ernst-Moritz-Arndt-University Greifswald, Germany.

Received: 23 April 2014 **Accepted:** 10 June 2014 **Available Online**: 30 June 2014

ABSTRACT

Tuberculosis (TB) is the leading cause of infectious disease related mortality worldwide. Infection of *Mycobacterium tuberculosis* (Mtb) leads to nearly 3 million deaths every year due to tuberculosis. Rifampicin and Isoniazid (RH) are the key drugs to being used for the treatment of tuberculosis. Reports in recent years indicate that the increasing emergence of resistance to these drugs. The resistance to these drugs severely affects options for effective treatment. The current vaccine for tuberculosis has variable protective efficacy and there is no commercially available serodiagnostic test for this disease with acceptable sensitivity and specificity for routine laboratory use, especially in case of multidrug resistance. In order to develop a new diagnostic tool for detection of Mtb, multidrug resistant Mtb as well and improve the tuberculosis vaccine, it is necessary to indentify novel antigenic candidates, especially in identification of multidrug resistant associated protein antigens. Here, we present a 2-D gel-based proteomic survey of the changes in RH resistant Mtb. The proteins extracted from RH resistant and susceptible Mtb clinical isolates were analyzed by two-dimensional differential in gel electrophoresis (2D-DIGE). Protein intensities of 41 spots were found to be regulated in RH resistant isolates. A total of 28 proteins were identified by matrix-assisted laser desorption ionization time-of-flight mass spectrometry. Twelve proteins of interest are NADH-dependent enoyl-[acyl-carrier-protein] reductase, 60 kDa chaperonin 2, Chaperone protein DnaK, 3-oxoacyl-(Acyl-carrier-protein0 reductase, Probable acetyl-CoA acyltransferase FadA2, two Acetyl/propionyl-CoA carboxylase, alpha subunit, Universal stress protein Rv1636/MT1672, Dihydrolipoyllysine-residue acetyltransferase component of pyruvate dehydrogenase complex, Glutamine synthetase 1 and two uncharacterized proteins (Rv2557 and Rv1505c).

Keywords: 2-D Differential in gel electrophoresis – 2D-DIGE; Mycobacterial proteomics; Mycobacteria, Tuberculosis; Multidrug resistance.

1. Introduction

Tuberculosis (TB) is the leading cause of infectious disease related mortality worldwide. Infection of *Mycobacterium tuberculosis* leads to nearly 3 million deaths every year due to tuberculosis. Multi-drug resistant strains, emergence of HIV-TB co-infection have increased the severity of tuberculosis epidemic. Multidrug resistance of tuberculosis leads to a serious threat in global tuberculosis control and treatment of patients seems to be impossible using currently available drugs. Multidrug resistant tuberculosis, associated with high death rates of 50-80%, spans a relatively short time from diagnosis to death [1]. Delayed detection of drug resistance could lead to an ineffective drug therapy and this could be one of the major factors contributing to multidrug resistant tuberculosis outbreaks. The emergence of multidrug resistant tuberculosis has increased interest in the understanding the mechanism of drug resistance in *M. tuberculosis* and the development of new therapeutics, diagnostics and vaccines.

The development of effective vaccines and rapid, simple, cheap test for the diagnosis is critical in the control and prevention of tuberculosis. The prevention of tuberculosis could be performed since 1921 by vaccination with Bacillus Calmette Guerin (BCG) vaccince. However, its efficacy continues to be debated. The basis of two meta-analyses of BCG vaccination demonstrated that the vaccine is efficient in preventing severe and life-threatening forms of tuberculosis in children [2]. Recently, several vaccine candidates including subunit vaccines have been developed and have entered clinical trials, and still more are in the pipeline of discovery [3-5].

***Corresponding author:** Truong Quoc Phong, Hanoi University of Science and Technology, Center for Research and Development in Biotechnology, No.1 Dai Co Viet, Hai Ba Trung, Ha Noi, Vietnam, Phone number: +84-36231457; Fax number: + 84-38682470; E-mail Address: phong.truongquoc@hust.edu.vn

The lack of powerful diagnostic procedure, especially diagnosis of multidrug resistant Mtb, leads to the difficulty in the control of this disease. Traditional tests based on the isolation and antibiotic sensitivity for diagnosis are time-consuming [6]. Several novel methods have been investigated and developed in recent years for diagnosis of tuberculosis such as nucleic acid amplification test, T-cell based assay, interferon gamma release assay and enzyme-linked immunospot assay [7-13]. However these methods require expensive equipments, a well-equipped and professional laboratory, highly trained personnel, and still time consuming. The utilization of these methods is limited in the developing countries where having a high proportion of *M. tuberculosis* infection. Enzyme-linked immunoabsorbent assay (ELISA), a simple, high throughput and inexpensive method, could be used for detection of *M. tuberculosis* infection [14].

Diagnosis of drug resistant tuberculosis plays an important role in the effective treatment. Early detection of drug resistance is one of the priorities of tuberculosis control. It allows initiation of the appropriate treatment and surveillance of drug resistance. Conventional phenotypic method for detection of drug resistance is based on detection of growth of *M. tuberculosis* in the presence of the antibiotics or indicator [2, 15-16]. However this method is time-consuming, therefore a new approach have been established for detection of drug resistance based on the analysis of DNA. This method has several advantages [2]. However, not all molecular mechanisms of drug resistance are known. Furthermore, drug resistance is due to mutation of several positions of target genes. Molecular characterization of rifampicin- and isoniazid resistant *M. tuberculosis* strains was performed and showed several mutation sites in the *rpoB* and *catG* gene. [17-19]. This method becomes more difficult in detection of multidrug resistance. Discovery of drug resistance consistently associated proteins of *M. tuberculosis*, especially multidrug resistance, could provide new biomarkers for detection using simple methods such as ELISA, lateral flow immunochromatographic assay.

Proteomics is a powerful tool for stuying the protein composition of complex biological samples. The proteomic approach along with *in vitro* and *in vivo* assessment of vaccine candidates can be very valuable in identifying new potential candidates in order to expand the antigenic repertoire for the development of effective novel vaccines against tuberculosis. The global study of the protein profile of resistant and susceptible strains by proteomic approach could help in further revealing of resistance mechanisms and determining multidrug resistance-associated biomarkers. The obtained findings support to develop newer drugs, development of vaccine and rapid diagnosis tool for multidrug resistance tuberculosis.

Investigations of protein expression profiles of *Mycobacterium tuberculosis* under various growth conditions, genetic backgrounds, geographic distribution have been performed [20-26]. Recently, researches on comparative analysis of drug resistant and suscetiple *Mycobacterium tuberculosis* by 2-DE combined with MS have been reported to reveal proteins associted with resistance [27-29].

Some studies in identification of biomarkers for serodiagnosis of drug resistant *M. tuberculosis* were performed by proteomic approach. Immunoproteome analysis of serum from patients infected with drug resistant or drug susceptible *M. tuberculosis* strains and heathy control identified three proteins as possible candidate biomarkers for use in the serodiagnosis of drug resistant tuberculosis infections [30]. Similarly, a proteome-scale identification of novel antigenic proteins in *M. tuberculosis* showed total of 249 proteins reacting significantly with the serum samples from patients in comparison with healthy cases [31].

The aim of this study was the comparison of the protein profiles of RH resistant and susceptible clinical *M. tuberculosis* isolates on the 2-D DIGE gel to identify RH resistant associated proteins.

2. Material and Methods

Mycobacterial growth

The RH resistant and sensitive *M. tuberculosis* clinical isolates (n = 3 per group to minimize genetic background differences) were obtained from National Institute of Hygiene and Epidemiology. Bacteria were grown in Middlebrook 7H12 broth at 37°C for four weeks (10^7-10^8 cfu/ml).

Sample preparation for proteomics

Mycobacterial cell extract was prepared according to modified protocol of as described [28]. Briefly, cells were washed three times with phosphate saline buffer (1X PBS buffer, pH 7.4) and then suspended in extraction buffer containing 8 M urea, 2 M thiourea, 2% CHAPS (Sigma-Aldrich, USA). The cell suspension was broken by intermittent sonication (15 seconds ON, 15 seconds OFF) for 4 min on ice at 80% energy using sonicator (Sonics & Materials Inc, USA). Subsequently, the lysate was clarified by centrifugation at 16,000 x g for 1 hour at 4°C. The supernatant was collected in a new eppendorf tube and protein concentration of the supernatant was determined using a Bradford assay kit (Sigma-Aldrich, USA). Sample aliquots were stored at -80°C for later use.

Two-dimensional differential gel electrophoresis (2-D DIGE)

Protein extracts (n = 3 per group) and a pooled internal standard containing aliquots of all isolate samples were labeled prior to electrophoresis with CyDyes according to the manufacture' recommendation (GE Healthcare). Briefly, 50 µg aliquots of each protein sample derived from each group was minimally labeled with 400 pmol of either Cy3 or Cy5 and the Cy2 dye was used for the labeling of the internal standard sample. The mixtures were incubated on ice for 30 min in dark followed by adding of 1 µl of 10 mM lysine for

quenching.

For 2-DE, two labeled samples (Cy3 and Cy5, each 50 µg) and the corresponding internal standard (Cy2, 50 µg) were mixed in rehydration buffer (8 M urea, 2 M thiourea, 2% CHAPS, 40 mM DTT, 0.6% Biolytes, pH 3-10 and trace of Bromophenol blue). Isoelectric focusing (IEF) was carried out using the method of in-gel rehydration [32]. Immobilized pH gradient strips of pH 4-7 and length 18 cm (Bio-rad, Hercules, CA, USA) were rehydrated overnight at 20°C with 150 µg labeled protein mixture. Strips were then focused on an IEF unit PROTEAN i12 IEF Cell (Bio-rad, Hercules, CA, USA) at 20°C using the following program: 250 V for 30 min in rapid mode, 10000 V for 2 h in gradual mode, 10000 V in rapid mode until 43 kVh reached and finally hold at 1000 V. The current limit was set at 50 µA per strip. After first dimension electrophoresis, IPG strips were equilibrated in buffer A (6 M urea, 0.375 M Tris, pH 8.8, 4% SDS, 20% glycerol and 1% DTT) for 15 min followed by equilibration in buffer B containing 2.5% iodoacetamide instead of DTT for further 15 min.

Separation of proteins on 12% SDS-polyacrylamide gels as the second dimension was performed [32] in a vertical electrophoretic dual gel unit PROTEAN II Xi (Bio-rad, Hercules, CA, USA) at constant power of 2 W for 16 hours. Images of the three different channels were acquired using a PharosFX Plus laser scanner (Bio-rad) at excitation/emission wavelength of 488/530 nm (Cy2), 532/605 nm (Cy3), and 635/695 nm (Cy5).

Spot detection, quantitation and statistical analysis

After scanning, analysis of the 2-D gel images was performed with the PDQuest Advanced software package version 8.0.1 (Bio-rad, Hercules, CA, USA). Images were analyzed using stepwise spot detection. Spot volumes were calculated based on the area and pixel intensities of spots. These spot volumes were normalized by a two-step procedure. In the first step, interchannel and intergel differences (Cy3, Cy5 and Cy2) in the intensities were corrected by dividing the background corrected values of the spot volumes by median of all spots of the channel (Cy2, Cy3 and Cy5). Then, fluorescence intensities of each spot were calibrated with the internal standard (Cy2) by dividing the median normalized spot volumes of the Cy3- and Cy5-channels by their correcting spot value of the Cy2 channel. The mean relative spot volumes of the group were used to reveal resistant-dependent changes in protein spot volumes by determining the ratios of the mean relative spot volumes between the susceptible and resistant group. We predefined stringent selection criteria in order to minimize the number of false positive results and defined the change in the level of a protein spot as significant only when the following two criteria were fullfilled: (i) the change in the intensity ratio between two groups had to exceed a factor of 1.5; (ii) the p-value of the corresponding Student's t-test had to be lower than 0.05. Resultant composite images for susceptible and resistant isolates were manually checked for artifactual spots, merged spots and missed spots.

Matrix assisted laser desorption ionization time-of-flight tandem mass spectrometry (MALDI-TOF-MS/MS)

In order to identify proteins from spots showing significant differences in intensities, spots of interest from colloidal coomassie brilliant blue stained gels of protein extracts pooled from all isolates were manually excised and subsequently subjected to mass spectrometry for identifications. Preparation of peptide extracts and MALDI-TOF mass spectrometric analysis on a Proteome Analyzer 4800 (Applied Biosystems, Darmstadt, Germany) were carried out as described previously [32]. Identification of proteins was based on peptide mass fingerprint (PMF) data confirmed by at least one protein specific peptide fragmentation pattern. Identification with the UniProtKB/ Swiss-Prot database for *Mycobacterium tuberculosis* using the MASCOT algorithm via the GPS Explorer software (Applied Biosystems) were considered to be statistically significant when the protein and peptide ion scores exceeded 49 and 16, respectively, which corresponds to $p<0.05$. Mass tolerances for precusor ions and for fragment ions were 50 ppm and 0.45 Da, respectively. Methionine oxidation was set as variable and carbamidomethylation as fixed modification.

3. Results

Proteome reference map of Mycobacterium tuberculosis clinical isolates

In order to provide a baseline of the proteome of clinical *Mycobacterium tuberculosis* isolates and to define the functional classes of identified proteins, a proteome reference map was constructed. Total protein extracts from RH resistant and susceptible clinical *Mycobacterium tuberculosis* isolates were separated by 2-DE, visualized with a colloidal coomassie brilliant blue staining and 96 spots corresponding to the most abundant proteins were excised. After tryptic digestion, peptide mixtures were subjected to MALDI-TOF MS/MS for protein identification. A total of 79 proteins were identified (Supporting information Fig. S1 and Table S1). The majority of spots (91%) contained only one protein and 7 spots contained two proteins. Using the PANTHER (Protein Analysis Through Evolutionary Relationships at http://www.pantherdb.or) classification software, the identified proteins were assigned to biological processes (Fig. 1). Classification of identified proteins showed the most prominent categories belonging to metabolic process (47%), response to stimulus (9%), immune system process (9%).

Quantitative comparative proteome profiling of the susceptible and RH resistant isolates by 2-D DIGE

In order to identify changes in protein abundance in re-

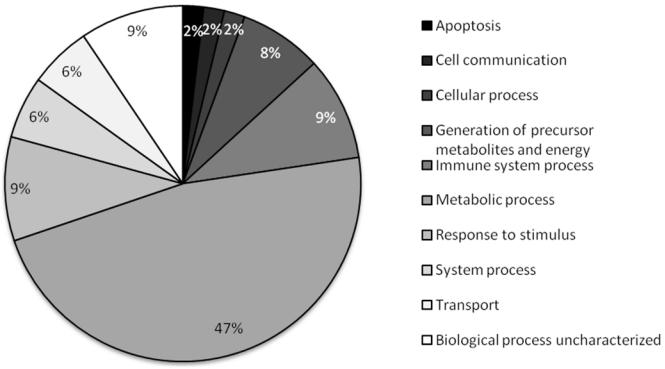

Figure 1. Functional classification of proteins of the clinical *Mycobacterium tuberculosis* reference map. Proteins were assigned to functional categories by uploading the results of the protein identification to the PANTHER classification software. The pie chart represents the distribution of identified proteins according to biological processes.

sistant isolates with high confidence, we employed the 2-D DIGE technology pioneered by Unlu et al. [33]. Representative examples of images of protein patterns generated with this sample set are shown in Fig. 2. A visual inspection of the images indicates that the protein patterns of the different groups looked similar. Quantification of the spot volumes with the PDQuest software package generated a spot set of a total of 458 spots, which were analyzed throughout all 2-D gels included in the experiment.

For quantitative analysis, the normalized spot volumes of the different groups of isolates were used to reveal multidrug resistant-dependent changes in the level of proteins by determining the ratios of mean relative spot volumes between the susceptible and RH resistant group. With a minimum of 1.5 fold change in level and a p-value of the corresponding Student's t-test lower than 0.05, a total of 41 protein spots was shown to display multidrug resistant-associated changes in intensity. The increase in spot volume in multidrug resistance was more pronounced than reduction (Fig. 3). The majority of those displayed increased intensity (23 protein spots – 56%) and a smaller proportion (18 protein spots – 44%) exhibited multidrug resistant-associated reduction of intensity (Supporting information Table S2).

Representative magnified regions of regulated proteins are showed in Fig. 4. These protein spots were excised from gels and subjected to matrix-assisted laser desorption/ionization time-of-flight (MALDI-TOF) mass spectrometry

Identification of spots displaying RH resistant-associated changes in intensity

Analysis of the DIGE experiment indicated changed levels of proteins associated with RH resistance. In order to detect which proteins actually differ in amount, the corresponding protein spots were excised from gels. Spots of interest were digested with trypsin and subjected to analysis by MALDI-TOF MS. Twelve proteins of interest are NADH-dependent enoyl-[acyl-carrier-protein] reductase, 60 kDa chaperonin 2, Chaperone protein DnaK, 3-oxoacyl-(Acyl-carrier-protein0 reductase, Probable acetyl-CoA acyltransferase FadA2, two Acetyl/propionyl-CoA carboxylase, alpha subunit, Universal stress protein Rv1636/MT1672, Dihydrolipoyllysine-residue acetyltransferase component of pyruvate dehydrogenase complex, Glutamine synthetase 1 and two uncharacterized proteins (Rv2557/MT2634 and) (Table 1).

4. Discussion

Accurate quantitation of changes in protein expression remains one of the most important aspects of proteomics. Conventional 2-D PAGE with Coomassie Brilliant Blue or silver staining followed by image analysis is limited by the sensitivity and dynamic range of these detection methods [34,35]. 2-D Fluorescence Difference Gel Electrophoresis (2-D DIGE) is a method to label proteins with CyDye fluors

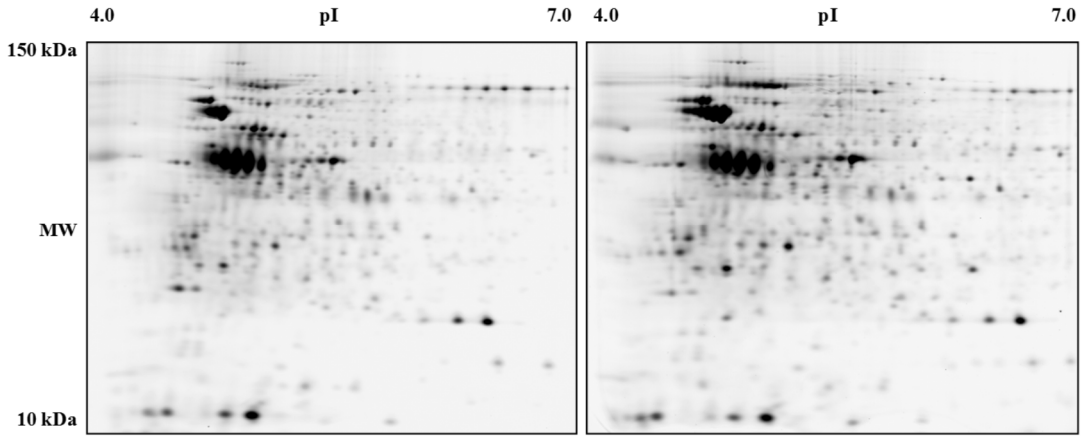

Figure 2. Protein patterns of susceptible and resistant clinical isolates of *Mycobaterium tuberculosis*. Protein samples were subjected to DIGE as described in Section 2. The images display representative examples of protein profiles of susceptible (A) and RH resistant isolates (B).

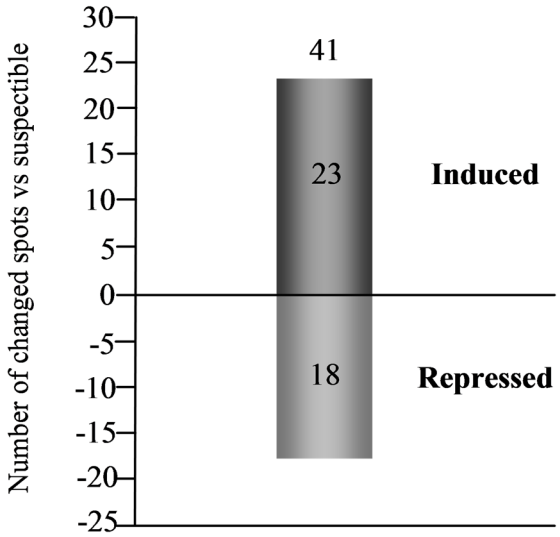

Figure 3. Bar graphs of protein spots displaying RH resistant-associated changes in intensity. Protein spot intensities were quantified and normalized to the internal standard using PDQuest software as above described. Protein display at least a 1.5 fold changes between the mean values of RH resistant isolate group compared to susceptible isolate group were considered as significant changed.

that are subsequently separated using 2-dimensional gel electrophoresis. This technology allows the separation of up to three different protein samples in the same 2-D gel because each of the three protein samples is labeled with one CyDye. The different labeled samples will be subjected to exactly the same 1st and 2nd dimension running conditions so the same protein labeled with a CyDye will migrate to the same position on the 2-D gel, this helps limit experimental variation. The multiplexing ability of DIGE experiment using an internal standard ensures correct co-identification of protein spots within the gel and accurate quantitation of expression differences. Thus, the technique is highly sensitive with a wide dynamic range for detection of proteins and compatible with state-of-the-art protein identification techniques using mass spectrometry. Comparative protein expression profiling is best performed with DIGE experiment [36,37].

In the present study we have applied the DIGE technique coupled with mass spectrometry for the identification of changed proteins in RH resistant *M. tuberculosis* isolates compared to RH susceptible isolates. The two-dimensional electrophoresis protein patterns of RH resistant and susceptible groups of *M. tuberculosis* isolates were highly similar (approximately 91% homology). This observation was coincided with the previous research [27,28]. A total of 17 distinct proteins of all 41 regulated protein spots were identified by mass spectrometry.

Protein spots 1 and 2 were up-regulated in RH resistant *M. tuberculosis* isolates and identified as chaperone protein DnaK (heat shock 70 kDa protein) and 60 kDa chaperonin 2 (GroEL-2), respectively. Chaperones in particular heat shock protein play an essential role in the maintenance of living ability of the cell. They are proteins to assist nascent proteins to reach right fold, protect subunits from heat shock during the assembly of complexes, prevent protein aggregation or mediate targeted unfolding and disassembly. Up-regulation of these proteins in response to stress is a key factor in the health of the cell and life-span of an organism [38]. DnaK assists the folding of several proteins. Unfolded proteins are transferred to another chaperone, the barrel-shaped GroEL - a highly specialized folding machine. This complex forms a nano-cage in which a single protein chain is temporarily enclosed and allowed to fold while protected from external influences [39].

DnaK has characteristic peptide binding domain and ATPase domain, which indicate its role in active protein refolding and proper assembly. Functional categories of DnaK were related to virulence, detoxification and adaptation [40]. Based on reference map, the distribution of DnaK

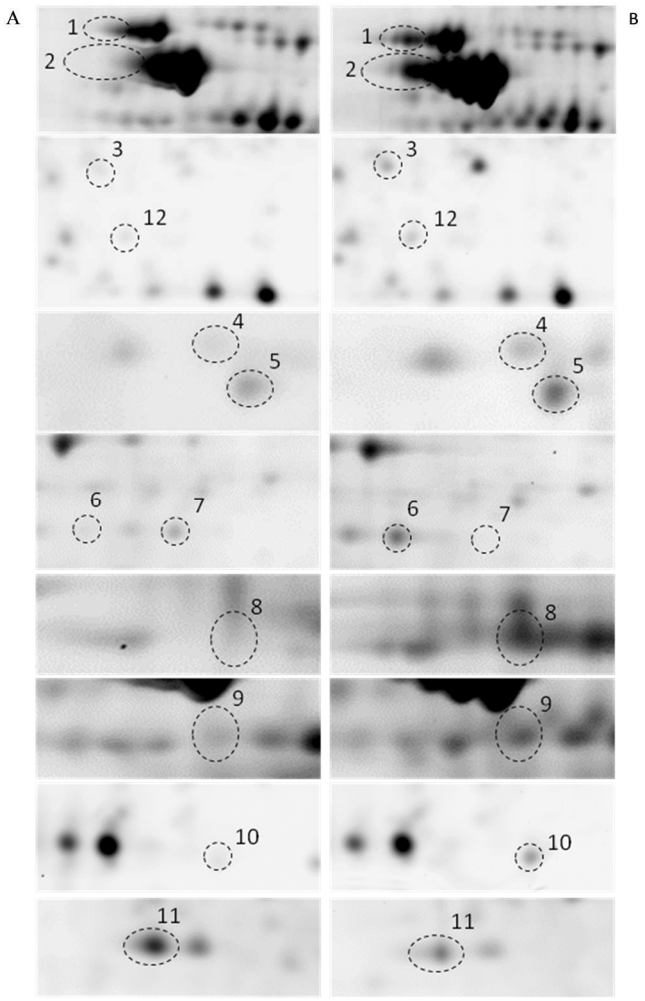

Figure 4. Representative magnified regions of 2-D gels showing the regulated proteins in comparison between the susceptible isolates (A) and RH resistant isolates (B).

Table 1. Identification of regulated proteins by MALDI-TOF mass spectrometry in RH resistant *Mycobacterium tuberculosis* isolates.

Spot No.	Regulated (p-value)	Accession No.	Proteins identified	Mass (Da)	pI	Score	Ions score	Sequence coverage (%)	No. of peptides matched
1	1.75 ↑ (0.00376)	DNAK_MYCTU (Rv0350)	Chaperone protein DnaK	66831	4.59	478	377.9	36.32	15
2	2.24 ↑ (0.01671)	CH602_MYCTU (Rv0440)	60 kDa chaperonin 2	56727	4.56	359	225.3	48.89	17
3	1.67 ↑ (0.03186)	INHA_MYCTU (Rv1484)	Enoyl-[acyl-carrier-protein] reductase [NADH]	28528	6.02	157	123	33.09	7
4	1.56 ↑ (0.00822)	L7N5J4_MYCTU (Rv0243)	Probable acetyl-CoA acyltransferase FadA2 (3-ketoacyl-CoA thiolase) (Beta-ketothiolase)	46107	6.64	659	576.9	43.18	11
5	1.85 ↑ (0.00975)	O53665_MYCTU (Rv0242c)	3-oxoacyl-(Acyl-carrier-protein) reductase	46830	6.38	656	441.6	63.00	23
6	1.68 ↑ (0.00502)	L7N4G3_MYCTU (Rv3285)	Acetyl/propionyl-CoA carboxylase, alpha subunit	63783	5.51	590	375.5	58.83	26
7	1.82 ↓ (0.00830)	L7N4G3_MYCTU (Rv3285)	Acetyl/propionyl-CoA carboxylase, alpha subunit	63783	5.51	504	327.5	49.83	23
8	1.63 ↑ (0.03373)	ODP2_MYCTU (Rv2215)	Dihydrolipoyllysine-residue acetyltransferase component of pyruvate dehydrogenase complex	57088	4.64	237	166.2	33.27	12
9	1.53 ↑ (0.02786)	GLNA1_MYCTU (Rv2220)	Glutamine synthetase 1	53570	4.84	257	173.6	41.42	13
10	1.73 ↑ (0.01660)	Y1636_MYCTU (Rv1636)	Universal stress protein Rv1636/MT1672	15312	5.62	225	152.2	80.14	8
11	1.69 ↓ (0.00021)	Y2557_MYCTU (Rv2557)	Uncharacterized protein	24295	4.54	296	175	72.32	14
12	1.54 ↑ (0.01525)	L0T720_MYCTU (Rv1505c)	Uncharacterized protein	24056	5.97	151	95.7	42.53	7

in the 2-D gel pattern tends to shift pH toward the acidic end of the IPG strip, suggesting that the identified spot was the result of posttranslational modifications (Fig. 3). This phenomena was observed with spot 2, identified as 60 kDa chaperonin 2 (GroEL-2) (Fig.3). GroEL-2 was identified in vitro as the most prominently phosphorylated proteins by PknJ [41] and this protein has been considered as the substrate of STRKs [42]. Therefore, the pI shift of this protein toward the acidic end may be due to phosphorylation. This protein was also known as heat shock protein 60, heat shock protein 65, 65 kDa antigen, cell wall protein A, antigen A [43]. As a chaperone, function of this protein was suggested to prevent misfolding and promote the refolding and proper assembly of unfolded polypeptides generated under stress conditions. This protein was predicted to a specialised regulation in *M. tuberculosis* because the location of this gene in *M. tuberculosis* genome is away from classic GroEL-Cpn10 operon [28]. As an antigen the *M. tuberculosis* heat shock protein 60 plays also an important role in modulating immune response of T-cell and macrophage [44,45]. Furthermore, it is noteworth that an increase of this protein was also found at the lower spot on 2-D gel. This observation indicated that the identified spot was a proteolytic degradation product of original protein. Recent study demonstrated that proteolysis of this protein could provide a potential source of immunogenic peptides in human tuberculosis [46]. A DNA vaccine based on this protein was demonstrated to activate human immune response [3]. Therefore this protein is considered as a candidate antigen for development of a subunit vaccine against mycobacteria. Furthermore, these proteins have also been reported to be up-regulated in drug resistant *M. tuberculosis* strains [28,29], suggesting that overexpression of these proteins might be accompanied with the drug resistance of mycobacteria.

The *inhA* gene of *M. tuberculosis* has been proposed to encode the primary target of the antibiotic isoniazid (INH). Overexpression of InhA in mycobacteria results in a 20-fold increase in the minimum inhibitory concentration of INH [47,48]. Resistance to INH might the result from drug sequestration by this protein. Furthermore, NADH-dependent enoyl-[acyl-carrier-protein] reductase was related to mycolic acid biosynthesis, an essential component of cell wall [49]. In

this study we found that this enzyme was significantly induced in abundance in RH resistant isolates. Therefore, it is possible that the increase of this enzyme improve the integrity of cell wall, ensuring the survival of mycobacteria whenever exposing to INH drug.

Another functional category of proteins that was significantly altered in abundance was related to the lipid metabolism. They were acetyl/propionyl-CoA carboxylase, alpha subunit, Probable acetyl-CoA acyltransferase FadA2, 3-oxoacyl-(Acyl-carrier-protein) reductase. Unlike NADH-dependent enoyl-[acyl-carrier-protein] reductase, no evidence indicated that there was direct interaction between these enzymes and INH adducts. However, it is possible that these enzymes might play a role in the construction of mycobacterial cell wall through lipid metabolism. Mycobacterial cell wall is known as the primary permeability barrier responsible for resistance to antibiotics [50]

The *dlaT* gene (Rv2215) and *glnA1* genes were encoding for dihydrolipoyllysine acetyltransferase (DlaT) component of pyruvate dehydrogenase complex and glutamine synthase, respectively. They were found to be up-regulated in RH resistant isolates. DlaT was required to convert pyruvate to acetyl-CoA, which is central to the intermediary metabolism and respiration of *M. tuberculosis*. DlaT enzyme is together with AceE and Lpd enzymes to construct the pyruvate dehydrogenase [51] and the lack of DlaT enzyme was leading to the lost of pyruvate deghydrogenase activity and reduction of *M. tuberculosis* viability in the host. Furthermore, there was evidence indicating that the mutation of the *M. tuberculosis dlaT* gene resulted in the impossibility of significant pathology in infected animal [52]. Similarly, GlnA1 enzyme, an enzyme of central importance in nitrogen metabolism, was demonstrated as essential factor in the pathogenicity of *M. tuberculosis* [53]. Therefore, these enzymes are considered as an essential for pathogenesis of *M. tuberculosis* and thus inactivation of DlaT and GlnA1 enzymes by some ways might be a potential approach for tuberculosis therapy. It will become a potential target for development of newer drugs in tuberculosis treatment. Besides its essential role in intermediary metabolism and respiration, DlaT enzyme also involves in antioxidant defense of *M. tuberculosis* a long with AhpC, AhpD and Lpd, [54]. The increase of antioxidant activity in this case seems to be compensation of the lack of the KatG catalase-peroxidase activity reduced in many isoniazid resistant strains. There was the existence of evidence indicating that antioxidant and glutamine synthetase activity of *M. tuberculosis* play an important role in suppressing host immune responses, suitable for pathogenesis. A modified BCG vaccine with reduction of these activities showed improvement in vaccine safety and effectiveness [55]

In the present study a universal stress protein (Rv1636/MT1672) was found to be up-regulated in resistant isolates. This protein was belonging to iron-regulated universal stress protein family and also considered as a member of family of *M. tuberculosis* hypothetical proteins including Rv2005c, Rv2623, Rv2026c, Rv1996, with unknown function [56]. However, in generally the universal stress protein (Usp) is a small cytoplasmic bacterial protein whose expression is enhanced when the cell is exposed to stress agents. Usp enhances the rate of cell survival during prolonged exposure to such conditions, and may provide a general stress response activity.

5. Concluding Remarks

This study is the first report applying 2-D DIGE technique for comparative analysis of RH resistant and susceptible clinical *M. tuberculosis* isolates. Total of 41 proteins spots were found to be regulated in RH resistant isolates. Identified proteins from these spots were functionally classified into virulence, adaptation and lipid metabolism. These differentially expressed proteins from RH resistant isolates might be considered as candidates for development of novel vaccine and rapid diagnosis tool for multidrug resistant tuberculosis.

6. Supplementary material

Supplementary data and information is available at: http://www.jiomics.com/index.php/jio/rt/suppFiles/168/0

Supplementary Fig. S1 - Proteome reference map of *Mycobacterium tuberculosis* clinical isolates. Total extract of proteins was separated by 2-DE DIGE gel. The most abundant spots were excised and subjected into MALDI-MS/MS for protein identification
Supplementary table S1 - Protein identification of spots on 2-D-DIGE gel by MALDI-MS for generating proteome reference map of *Mycobacterium tuberculosis* clinical isolates
Supplementary table S2 - Multiple DIGE data

Acknowledgements

The research was supported by the National Foundation for Science & Technology Development (NAFOSTED), Vietnam.

References

[1] A. Rattan, A. Kalia, N. Ahmad, Emerg Infect Dis, 4 (1998) 195-209. doi: 10.3201/eid0402.980207

[2] J.C. Palomino, S.C. Leão, V. Ritacco, (2007). Tuberculosis 2007: From basic sience to patient care. 1st edition.

[3] L.H. Franco, P.F. Wowk, C.L. Silva, A.P. Trombone, A.A. Coelho-Castelo, C. Oliver, M.C. Jamur, E.L. Moretto, V.L. Bonato, Genet Vaccines Ther, 6 (2008) 3. doi: 10.1186/1479-0556-6-3

[4] M.D. Tameris, M. Hatherill, B.S. Landry, T.J. Scriba, M.A. Snowden, S. Lockhart, J.E. Shea, J.B. McClain, G.D. Hussey, W.A. Hanekom, H. Mahomed, H. McShane, The Lancet, 381 (2013) 1021-1028. doi: 10.1016/s0140-6736(13)60177-4

[5] T. Hoang, C. Aagaard, J. Dietrich, J.P. Cassidy, G. Dolganov, G.K. Schoolnik, C.V. Lundberg, E.M. Agger, P. Andersen,

PLoS One, 8 (2013) e80579. doi: 10.1371/journal.pone.0080579

[6] Am J Respir Crit Care Med, 161 (2000) 1376-1395. doi: 10.1164/ajrccm.161.4.16141

[7] E.M. Leyten, B. Mulder, C. Prins, K. Weldingh, P. Andersen, T.H. Ottenhoff, J.T. van Dissel, S.M. Arend, J Clin Microbiol, 44 (2006) 1197-1201. doi: 10.1128/JCM.44.3.1197-1201.2006

[8] D.I. Ling, L.L. Flores, L.W. Riley, M. Pai, PLoS One, 3 (2008) e1536. doi: 10.1371/journal.pone.0001536

[9] D. Menzies, Annals of Internal Medicine, 146 (2007) 340. doi: 10.7326/0003-4819-146-5-200703060-00006

[10] A. Nienhaus, A. Schablon, R. Diel, PLoS One, 3 (2008) e2665. doi: 10.1371/journal.pone.0002665

[11] M. Pai, Annals of Internal Medicine, 149 (2008) 177. doi: 10.7326/0003-4819-149-3-200808050-00241

[12] MMWR Morb Mortal Wkly Rep, 58 (2009) 7-10.

[13] G.H. Mazurek, J. Jereb, A. Vernon, P. LoBue, S. Goldberg, K. Castro, MMWR Recomm Rep, 59 (2010) 1-25.

[14] S.L. Zhang, J.W. Zhao, Z.Q. Sun, E.Z. Yang, J.H. Yan, Q. Zhao, G.L. Zhang, H.M. Zhang, Y.M. Qi, H.H. Wang, Q.W. Sun, Tuberculosis (Edinb), 89 (2009) 278-284. doi: 10.1016/j.tube.2009.05.005

[15] I.S. Johansen, V.O. Thomsen, M. Marjamaki, A. Sosnovskaja, B. Lundgren, Diagn Microbiol Infect Dis, 50 (2004) 103-107. doi: 10.1016/j.diagmicrobio.2004.04.001

[16] S. Rusch-Gerdes, G.E. Pfyffer, M. Casal, M. Chadwick, S. Siddiqi, J Clin Microbiol, 44 (2006) 688-692. doi: 10.1128/JCM.44.3.688-692.2006

[17] D. Hillemann, T. Kubica, R. Agzamova, B. Venera, S. Rusch-Gerdes, S. Niemann, Int J Tuberc Lung Dis, 9 (2005) 1161-1167.

[18] R. Johnson, E.M. Streicher, G.E. Louw, R.M. Warren, P.D. van Helden, T.C. Victor, Curr Issues Mol Biol, 8 (2006) 97-111.

[19] U. Kozhamkulov, A. Akhmetova, S. Rakhimova, E. Belova, A. Alenova, V. Bismilda, L. Chingissova, S. Ismailov, E. Ramanculov, K. Momynaliev, Jpn J Infect Dis, 64 (2011) 253-255.

[20] J.C. Betts, P. Dodson, S. Quan, A.P. Lewis, P.J. Thomas, K. Duncan, R.A. McAdam, Microbiology, 146 Pt 12 (2000) 3205-3216.

[21] J.C. Betts, P.T. Lukey, L.C. Robb, R.A. McAdam, K. Duncan, Molecular Microbiology, 43 (2002) 717-731. doi: 10.1046/j.1365-2958.2002.02779.x

[22] J. Mattow, U.E. Schaible, F. Schmidt, K. Hagens, F. Siejak, G. Brestrich, G. Haeselbarth, E.C. Muller, P.R. Jungblut, S.H. Kaufmann, Electrophoresis, 24 (2003) 3405-3420. doi: 10.1002/elps.200305601

[23] J. Starck, G. Kallenius, B.I. Marklund, D.I. Andersson, T. Akerlund, Microbiology, 150 (2004) 3821-3829. doi: 10.1099/mic.0.27284-0

[24] K.G. Mawuenyega, C.V. Forst, K.M. Dobos, J.T. Belisle, J. Chen, E.M. Bradbury, A.R. Bradbury, X. Chen, Mol Biol Cell, 16 (2005) 396-404. doi: 10.1091/mbc.E04-04-0329

[25] C. Pheiffer, J.C. Betts, H.R. Flynn, P.T. Lukey, P. van Helden, Microbiology, 151 (2005) 1139-1150. doi: 10.1099/mic.0.27518-0

[26] H. Malen, G.A. De Souza, S. Pathak, T. Softeland, H.G. Wiker, BMC Microbiol, 11 (2011) 18. doi: 10.1186/1471-2180-11-18

[27] X. Jiang, W. Zhang, F. Gao, Y. Huang, C. Lv, H. Wang, Microb Drug Resist, 12 (2006) 231-238. doi: 10.1089/mdr.2006.12.231

[28] P. Sharma, B. Kumar, Y. Gupta, N. Singhal, V.M. Katoch, K. Venkatesan, D. Bisht, Proteome Sci, 8 (2010) 59. doi: 10.1186/1477-5956-8-59

[29] B. Kumar, D. Sharma, P. Sharma, V.M. Katoch, K. Venkatesan, D. Bisht, J Proteomics, 94 (2013) 68-77. doi: 10.1016/j.jprot.2013.08.025

[30] L. Zhang, Q. Wang, W. Wang, Y. Liu, J. Wang, J. Yue, Y. Xu, W. Xu, Z. Cui, X. Zhang, H. Wang, Proteome Sci, 10 (2012) 12. doi: 10.1186/1477-5956-10-12

[31] Y. Li, J. Zeng, J. Shi, M. Wang, M. Rao, C. Xue, Y. Du, Z.G. He, J Proteome Res, 9 (2010) 4812-4822. doi: 10.1021/pr1005108

[32] E. Hammer, T.Q. Phong, L. Steil, K. Klingel, M.G. Salazar, J. Bernhardt, R. Kandolf, H.K. Kroemer, S.B. Felix, U. Volker, Proteomics, 10 (2010) 1802-1818. doi: 10.1002/pmic.200900734

[33] M. Unlu, M.E. Morgan, J.S. Minden, Electrophoresis, 18 (1997) 2071-2077. doi: 10.1002/elps.1150181133

[34] S.P. Gygi, G.L. Corthals, Y. Zhang, Y. Rochon, R. Aebersold, Proc Natl Acad Sci U S A, 97 (2000) 9390-9395. doi: 10.1073/pnas.160270797

[35] T. Rabilloud, M. Chevallet, S. Luche, C. Lelong, J Proteomics, 73 (2010) 2064-2077. doi: 10.1016/j.jprot.2010.05.016

[36] B. Chakravarti, S.R. Gallagher, D.N. Chakravarti, Curr Protoc Mol Biol, Chapter 10 (2005) Unit 10 23. doi: 10.1002/0471142727.mb1023s69

[37] R. Diez, M. Herbstreith, C. Osorio, O. Alzate, Frontiers in Neuroscience. 2-D Fluorescence Difference Gel Electrophoresis (DIGE) in Neuroproteomics, in: O. Alzate (Ed.) Neuroproteomics, CRC Press.Llc., Boca Raton (FL), 2010.

[38] http://scitechdaily.com/dnak-identified-as-key-player-of-protein-folding/

[39] H. Saibil, Nat Rev Mol Cell Biol, 14 (2013) 630-642. doi: 10.1038/nrm3658

[40] J.M. Lew, A. Kapopoulou, L.M. Jones, S.T. Cole, Tuberculosis (Edinb), 91 (2011) 1-7. doi: 10.1016/j.tube.2010.09.008

[41] http://www.ncbi.nlm.nih.gov/gene/886354

[42] G. Arora, A. Sajid, M. Gupta, A. Bhaduri, P. Kumar, S. Basu-Modak, Y. Singh, PLoS One, 5 (2010) e10772. doi: 10.1371/journal.pone.0010772

[43] M.J. Canova, L. Kremer, V. Molle, J Bacteriol, 191 (2009) 2876-2883. doi: 10.1128/JB.01569-08

[44] T.M. Shinnick, 167 (1991) 145-160. doi: 10.1007/978-3-642-75875-1_9

[45] N. Khan, K. Alam, S.C. Mande, V.L. Valluri, S.E. Hasnain, S. Mukhopadhyay, Cell Microbiol, 10 (2008) 1711-1722. doi: 10.1111/j.1462-5822.2008.01161.x

[46] S.A. Shiryaev, P. Cieplak, A.E. Aleshin, Q. Sun, W. Zhu, K. Motamedchaboki, A. Sloutsky, A.Y. Strongin, FEBS J, 278 (2011) 3277-3286. doi: 10.1111/j.1742-4658.2011.08244.x

[47] M.H. Larsen, C. Vilchèze, L. Kremer, G.S. Besra, L. Parsons, M. Salfinger, L. Heifets, M.H. Hazbon, D. Alland, J.C. Sacchettini, W.R. Jacobs, Molecular Microbiology, 46 (2002) 453

-466. doi: 10.1046/j.1365-2958.2002.03162.x

[48] A. Argyrou, M.W. Vetting, J.S. Blanchard, J Am Chem Soc, 129 (2007) 9582-9583. doi: 10.1021/ja073160k

[49] S.V. Ramaswamy, R. Reich, S.J. Dou, L. Jasperse, X. Pan, A. Wanger, T. Quitugua, E.A. Graviss, Antimicrobial Agents and Chemotherapy, 47 (2003) 1241-1250. doi: 10.1128/aac.47.4.1241-1250.2003

[50] C.E. Barry, K. Mdluli, Trends in Microbiology, 4 (1996) 275-281. doi: 10.1016/0966-842x(96)10031-7

[51] J. Tian, R. Bryk, S. Shi, H. Erdjument-Bromage, P. Tempst, C. Nathan, Mol Microbiol, 57 (2005) 859-868. doi: 10.1111/j.1365-2958.2005.04741.x

[52] S. Shi, S. Ehrt, Infect Immun, 74 (2006) 56-63. doi: 10.1128/IAI.74.1.56-63.2006

[53] M.V. Tullius, G. Harth, M.A. Horwitz, Infect Immun, 71 (2003) 3927-3936. doi: 10.1128/iai.71.7.3927-3936.2003

[54] R. Bryk, C.D. Lima, H. Erdjument-Bromage, P. Tempst, C. Nathan, Science, 295 (2002) 1073-1077. doi: 10.1126/science.1067798

[55] C. Shoen, M. DeStefano, C. Hager, K.-T. Tham, M. Braunstein, A. Allen, H. Gates, M. Cynamon, D. Kernodle, Vaccines, 1 (2013) 34-57. doi: 10.3390/vaccines1010034

[56] S.M. Hingley-Wilson, K.E. Lougheed, K. Ferguson, S. Leiva, H.D. Williams, Tuberculosis (Edinb), 90 (2010) 236-244. doi: 10.1016/j.tube.2010.03.013

JOURNAL OF INTEGRATED OMICS
A METHODOLOGICAL JOURNAL
HTTP://WWW.JIOMICS.COM

ORIGINAL ARTICLE | DOI: 10.5584/jiomics.v4i1.159

A Novel High Throughput High Content Analysis Assay for Intermediate Filament Perturbing Drugs

Joanna Chowdry[1], Gareth J. Griffiths[2], Rod P. Benson[2], Bernard M. Corfe*[1]

[1] Molecular Gastroenterology Research Group, Academic Unit of Surgical Oncology, Department of Oncology, The Medical School, Beech Hill Road, S10 2RX, UK; [2]Imagen Biotech Ltd, Alderly Edge, Cheshire, SK10 4TG, UK.

Received: 15 November 2013 **Accepted:** 29 June 2014 **Available Online**: 30 June 2014

ABSTRACT

Keratins are predominantly found in epithelial cells and form the intermediate filament (IF) component of the cytoskeleton. Depolymerisation of these filaments causes the cell to collapse and become more plastic. We have previously shown that short chain fatty acids may trigger depolymerisation of keratins through altered protein acetylation. Currently, there is no single functional assay for screening of the cytoskeleton. The aim of this study is to develop a high-throughput assay to quantify IF depolymerisation and to apply as a screen for IF-perturbing nutrients and drugs. Three treatments were used in a proof-of-principle study: the anti-fungal drugs griseofulvin and cordycepin (the former is known tosuppress microtubule growth, the latter induces abnormal mitosis by suppressing microtubule dynamics with concequent impact on IF organisation) and sodium butyrate, a histone deacetylase inhibitor which disrupts IF formation in cancer cells via post-translational modification of keratins.

Methods were optimised for cell fixation using methanol or formalin, permeabilising agents for Keratin (krt) 8 antibody dilution (triton-x100, digitonin and saponin) and blocking of non-specific binding prior to cell staining using BSA, after which High Content Analysis (HCA) was employed to quantify cell staining intensities by comparing co-occurrence of adjacent pixel intensities. Immunocytochemistry was used to identify Krt 8 intermediate filaments. Indicators of depolymerisation include Krt 8 fluorescence intensity, filamentousness or texture intensity, fibre spot count and fibre spot total area. All treatments resulted in significant decreases for texture intensity. Proof of Principle was established using a Z'calculation. Griseofulvin gave values falling between 0.5 and 1 indicating the assay is suitable for high-throughput work.

In conclusion, a HCA assay for intermediate filament integrity has been demonstrated, establishing proof of principle with griseofulvin, and cross-validating with two further treatments assayable using this method.

Keywords: IF depolymerisation assay; Keratin 8; High content analysis; Proof of principle.

Abbreviations

Krt: keratin; **IF**: intermediate filament; **HCA**: high content analysis; **BSA**: bovine serum albumin; **K**: Lysine residue; **RPMI**: Roswell park memorial institute; **PBS**: phosphate buffered saline; **HPACC**: Health protection agency culture collections; **PTMs**: post translational modifications; **HDACi**, histone deacetylase inhibitor; **SCFAs** short chain fatty acids.

1. Introduction

Intermediate filaments (IFs) are found in all cells, with keratins particulary abundant in epithelial cells. They cross-link to microtubules, actin and myosin by accessory proteins such as filaggrin and plectin and bundle into strong arrays[1]. In contrast to microfilaments and microtubules, it is not understood how IFs remodel the cytoskeleton. By identifying keratins and keratin-associated protein mutations in disease, an insight can be provided into how they act. IFs confer rigidity to epithelial cells, characterised by high visco-elasticity and flexibility [2]. functioning to protect epithelial cells from mechanical and non-mechanical stress [3]. Interfering with the dynamics of IFs leads to a reduced resilience of the epi-

***Corresponding author:** Dr Bernard Corfe, Department of Oncology, University of Sheffield Medical School, Beech Hill Road, Sheffield S10 2RX, UK; Tel 44 114 281 3004; Fax 44 114 271 3314; **E**-mail address**:** b.m.corfe@sheffield.ac.uk.

thelia to mechanical stress [4].The highly dynamic keratin network implicates a perpetual cycle of assembly and disassembly commencing with nucleation of keratin particles at the cell periphery into a proto-filament, followed by elongation towards the nucleus to form a stable network. Perinuclear disassembly releases soluble oligers which diffuse through the cytoplasm and are recycled into new protofilaments at the periphery [4]. Intermediate filaments are formed from polymerised coiled dimers of Type I smaller acidic Krt 9 to 20 and Type II larger basic Krt 1 to 8 [5], comprising mainly Krt 8 and Krt 18 in intestinal epithelia). . Keratin regulation occurs through post translational modifications (PTMs). Krt 8 has been shown to be acetylated at five lysine residues: K10, K100, K392, K471 and K482 in HCT116 colon cancer cells [6] . Over-expression of Krt 8 has been implicated in several colorectal pathologies [7]suggesting that keratins may be essential to epithelial homeostasis and altered function may contribute to conditions such as inflammatory bowel disease[6].

HCA enables quantification of staining intensities by use of computational analysis of images captured by an automated fluorescent microscope adapted to read 96 well plates [8]. It is capable of measuring multiple cellular parameters simultaneously on a cell by cell basis and can also be used for semi-quantification of antibody staining profiles. The automation of acquisition and analysis means that the technique is high throughput and multi-parametric. We have previously employed HCA to analyse the effects of short chain fatty acids on Krt 8 acetylation [9] and cytoskeletal structure [8], demonstrating that butyrate-induced acetylation of Krt 8 is associated with reduced polymerisation of IFs [9]. The benefits of HCA include substantial cost savings due to a reduction in the number of hours involved in performing the experiment and smaller amounts of consumables being used. In drug development, HCA streamlines the work load required for validating drugs prior to animal and clinical testing as well as supplementing systems biology [8].

Currently, there exists no keratin screening tool in a single functional assay. The aim of this study is to establish a viable assay for cytoskeletal staining of intermediate filaments, and to establish proof of principle for high throughput development following perturbation with depolymerising agents.

2. Material and Methods

2.1 *General Reagents and Solutions*

Phosphate-buffered saline Dulbecco "A" (PBS) solution was supplied by OXoid, Basingstoke, U.K. RPMI1640 GlutaMAX media was supplemented with 500 units of penicillin/streptomycin and L-Glutamine 2 mM final conc (Gibco Life Technologies, Invitrogen, U.K) and 10 % Foetal Bovine Serum (Biosera, East Sussex, U.K). The cell treatments griseofulvin, cordycepin and sodium butyrate were supplied by Sigma-Aldrich, Poole, Dorset, U.K. Cells were stained with mouse monoclonal antibodies to Krt 8 supplied by abcam, Cambridge, U.K and Alexafluor 555 donkey anti mouse antibody and Hoechst 33342 weresupplied by Invitrogen, U.K.

2.2 *Cell Culture protocol*

MCF-7 cells obtained from HPACC were cultured in RPMI media and incubated at 37 °C, 5% CO_2 in humidified air. Confluency, viability and cell counts (stained with Trypan Blue, Gibco, Life Technologies, U.K,) were assessed using an optical microscope and haemocytometer ("Improved Neubauer" chamber).

2.3 *Protocols for High Content Analysis (HCA):*

Cell Seeding and Treatment

MCF-7 cells were cultured in Black-sided Costar 96-well culture plates (Sigma-Aldrich) at 2.5 x 10^3 cells per 100 µl RPMI media. Plates were incubated at 37 °C for 24 hours to allow cells to adhere, after which media was replaced with fresh media containing either sodium butyrate treatment at 0, 2.5, 5, 10, 15, 20 mM for 16 hours, n = 20 for initial pilot experiment to optimise staining conditions, griseofulvin in at 0, 2, 5, 10, 20, 50, 100, 150 and 200 µM for 48 hours (n = 3), or cordycepin, (0, 2, 5, 10, 15, 30 and 60 µM for 15 and 30 minutes, n = 3),the latter two containing 0.1% DMSO to aid solubilisation with relevant vehicle only controls.

Optimisation of Staining

Preliminary experiments were undertaken with 20 mM Sodium Butyrate to optimise staining, fixing and blocking protocols, as detailed below.*Fixative:* Cells were fixed with either 10 % buffered formalin (Sigma-Aldrich) for 15 minutes at room temperature, or ice cold methanol (Fisher Scientific, Loughborough, U.K) for 5 minutes at minus 20 ° C, after which, they were washed twice with 100 µl PBS before a final addition of 100 µl PBS. Plates were sealed for storage at 4 °C prior to staining.

Blocker: Prior to antibody staining, plates were blocked for non-specific protein binding with either PBS control or 2% BSA (made up in PBS) for 10 minutes to observe differences in background staining intensities as well as differences in texture and fluorescence intensity.

Permeabilisation: To facilitate entry into the cell, the antibody was diluted in a detergent or permeabilising agent according to Cellomics' HCA protocols. Mouse monoclonal Krt 8 antibody was diluted at a final concentration of 0.01 mg/ml in PBS containing 500 µg/ml digitonin, or 1 mg/nl saponin or 0.1% triton X-100. 50 µl of antibody was added to each well and left for 1 hour at room temperature. Wells were washed three times with 100 µl PBS and subsequently stained for 30 minutes at room temperature with 50 µl of 0.005 mg/ml Alexafluor red 555 donkey anti-mouse antibody containing 0.004 mg/ml Hoechst 33342 DNA stain. As before, wells were washed three times with 100 µl PBS, with a

final addition of 100 µl PBS to store the cells in. Plates were sealed and stored at 4 °C prior to image analysis.

HCA Image Analysis and Quantification

Analysis was undertaken using a Cellomics Arrayscan II platform which employs a Compartmental Analysis algorithm for measurement of total cytoplasmic fluorescence intensity (arbitrary units) [8]. A morphology algorithm enables cell texture intensity measurements (arbitrary units) to be determined, based on the co-occurrence of adjacent pixel intensities. This is derived from the probability of pixels with different intensities occurring next to each other. Co-occurence measures how filamentous the cytoskeleton is. A strong healthy protein is visualised as rough filaments whereas a broken protein causes filaments to become 'mushy' with a smooth, diffused appearance,. This non-filamentousness, consistent with cellular depolymerisation, is characterised byuniform staining, providing a low texture intensity measurement .Highly varied intensities indicate structural staining, providing a larger value for this parameter. The contrast measurement reflects the strength of occurences of pixels of differing intensity being adjacent to each other, whereby the greater the difference, the stronger the weighting. Other parameters measured included cell count (per well), fibre spot count and fibre spot total area (arbitrary units). The method for fibre-spot size analysis identifies which pixels belong to spots or fibres by evaluating the change in intensity over space within the object. A background correction is applied automatically to differentiate between spots and fibres, and intra-cellular noise [10].

3. Results and Discussion

Optimisation of Intermediate Filaments Staining for HCA

Both methanol and formalin fixation were used to assess the viability of developing a dual assay for keratin/tubulin or keratin/actin staining. Methanol is traditionally employed in immunofluoresence experiments as the fixative of choice for microtubules and intermediate filaments since cross-linking reagents such as formaldehyde, though good at preserving cell structure, may reduce antigenicity of components [11]. Preliminary experiments of cells treated with sodium butyrateshowed that methanol fixation provided consistently sharper images (Fig 1, panel 2) compared to 10% formalin (Fig 1, panel 1). Additionally, cells treated with increasing concentrations of butyrate and fixed with methanol remained consistent in number compared to those fixed with formalin which showed a reduction in cell count, P <0.005 (Fig 1D, expressed as percent of control population), hence methanol was used as a fixative of choice.

An initial 30 minute blocking step with BSA (2 %) was included to block non-specific binding of the Krt 8 antibody (Fig 1A - 1C, panels 1 and 2). Visual inspection of acquired images showed no major difference between PBS control or BSA blocked cells. No significant difference was observed in texture intensity measurement when comparing unblocked (PBS) cells to 2% BSA blocked cells using a students paired T test (PBS 1.07 ± 0.62 vs 2% BSA 1.09 ± 0.63, P = 0.86, arbitrary units) or Krt 8 mean total fluorescence intensity (PBS $3.6 \times 10^6 \pm 2 \times 10^6$ vs 2% BSA $3.3 \times 10^6 \pm 1.9 \times 10^6$, P = 0.44, arbitrary units). Consequently this step was omitted in future experiments enabling mechanical manipulations to be kept to a minimum, thus ensuring the quality of final images would remain uncompromised.

Intracellular epitopes require permeabilising to allow the

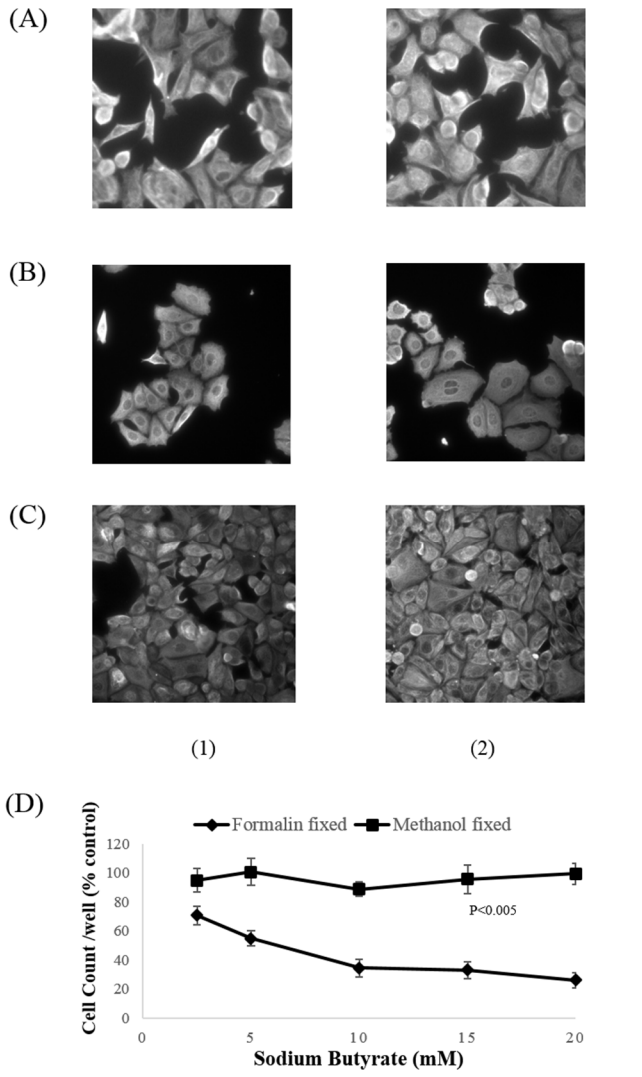

Figure 1. *A comparison of fixation methods on MCF-7 cells* (x20 magnification) treated with 20 mM sodium butyrate using (1) 10% formalin, (2) methanol. (A) No blocker, Krt 8 antibody diluted with PBS (B) No blocker, Krt 8 antibody diluted with 1mg/ml saponin, (C) 2% BSA blocker, Krt 8 antibody diluted with 1mg/ml saponin and (D) Effect of formalin (10%) vs methanol fixation on MCF-7 cell count per well expressed as a percent of control (n = 20, mean ± SEM) following sodium butyrate treatment (0 – 20 mM)

antibody to access the inside of the cell to detect the protein of interest. Low concentrations of Triton X-100 has been shown to remove some cortical fluorescence from mitotic cells [12], where detergent-resistant material was identified as non-filamentous keratin aggregates. Drake et al [8] and Khan et al [9] diluted antibodies with a digitonin permeabilising solution in accordance with Cellomics' HCA internal protocols. In preliminary experiments using sodium butyrate, cells stained with Krt 8 antibody at a concentration of 0.01 mg/ml diluted in PBS (Fig 1A) or 0.1 % Triton X-100 did not stain as well as those using the milder membrane solubilisers digitonin (500 μg/ml) and saponin (1 mg/ml), the latter two thought to produce pores sufficiently large enough for the antibody to pass through without dissolving the plasma membrane. On closer visual inspection, saponin showed better uniform staining of cellular architecture and was used in subsequent experiments (Fig 1B, 1C).

Assay validation with intermediate filament disrupting agents.

All cytoskeletal components are co-ordinated – no part acts alone. Drugs affecting actin, tubulin, or both may also affect the intermediate filament organising system. Interference of intermediate filament dynamics in human disease and transgenic mice leads to reduced resilience of the epithelia to mechanical stress [4]. Gordon et al [13] demonstrated disruption of microtubules, but not actin, could lead to intermediate filament reorganisation. Effects of the cytostatic drugs cytochalasin B, D and β lumicochicine and vinblastine on microtubules and microfilaments showed an induction of keratin rearrangement in Hela cells [14]. SW13 cells treated with latrunculin B (destroys actin) and nocozadole (depolymerises microtubules) completely blocked keratin motility, implying that this function relies both on intact actin microfilaments and microtubules [15].

Following an extensive knowledgebase review, griseofulvin was identified as a potent trigger of intermediate filament breakdown. A metabolic product of *Penicillium griseofulvium*, griseofulvin is absorbed by the GI tract into body fluids and tissues eventually reaching keratinised skin structures [16]. Griseofulvin-damaged mouse livers incorporated with ^{32}P orthophosphate showed alterations in keratin filament architecture where a shift towards acidic isoforms of Type I keratins was thought to be due to hyperphosphorylation [17], demonstrating the role PTMs play in IF homeostasis *in vivo*. This C-mitotic anti-fungal drug induces G2-M arrest / apoptosis in several cell lines, selectively killing cancer cells yet sparing healthy cells [18]. MCF-7 cells treated with 15 - 90 μM griseofulvin for 24 – 48 hours stabilised microtubule dynamics by reducing the length and rate of growing and shortening phases [19]. For this reason, griseofulvin was chosen as an IF perturbing tool in the current studies to evaluate its effect on cytoskeletal depolymerisation.

The adenosine analogue Cordycepin, deriving from culture filtrates of *Cordyceps militaris* and *Aspergillus nidulans*, was the first naturally occurring nucleotide (3'-deoxyadenosine) to be isolated [20]. Zeive et al [21] demonstrated rapid collapse of intermediate filaments in keratinocytes treated with cordycepin where microtubules were depolymerised to small stumpy asters. MCF-7 cells treated with cordycepin suggested the initial effect on cell cycle was due to changes in polyadenylate polymerase activity prior to apoptosis [22]. OEC-M1 cells treated with cordycepin and stained with annexin V for early apoptosis appeared rounded up after 3 hours but were still adherent to the matrix (longer treatments of up to 48h reflected an apoptotic trend thought to be cordycepin inducing G2/M cell arrest [23]). Low doses have been shown to decrease cell proliferation whereas high doses affect cell adhesion and indirectly reduce protein synthesis [24]. Inhibition of MCF-7 cell proliferation by cordycepin has been attributed to autophagy rather than apoptosis [25]. As a result of these findings, cordycepin was identified as a potential candidate for IF disruption in this proof of principle study.

The short chain fatty acid sodium butyrate was chosen for preliminary experiments. The most biologically potent of the SCFAs, it has previously been shown to strongly effect cellular depolymerisation prior to apoptosis [8], making it an ideal candidate for optisation of staining protocols. It is naturally produced in the colon by fermentation of dietary fibre and is a fuel for colonocytes. Colon carcinoma cell proliferation is inhibited via early G1 phase arrest at concentrations of 1 -5 mM sodium butyrate with no impact on cell viability (proliferation is stimulated in normal colonic epithelium) [26] and induces apoptosis *in vitro*. Hela cells incubated with 1 – 5mM butyrate increased histone acetylation by inhibiting histone deacetylase, paralleling changes seen in H3 phosphorylation [27]. Multiple sites of acetylation in Krt 8 and Krt 18 have been identified by our group [8] in HCT116 and CaCo2 cells, where butyrate-induced acetylation of Krt 8 was associated with breakdown of the cytoskeleton via reduced polymerisation of IFs [9]. Immuno blots of intermediate filaments isolated from butyrate treated HCT116 cells treated further confirm Krt 8 is acetylated, thus conveying the HDACi status of butyrate as a post translational modifier of cytokeratins [6].

Proof of Concept as a high-throughput assay

Assay efficacy was established and validated by using the proof of principle Z' calculation to acertainwhether the response was sufficient enough to warrant further investigation. Acceptable Z' values fall between 0.5 and 1.0, with perfect assay values approaching 1.0 [28].

MCF-7 cells treated with 100 μM griseofulvin for 48 hours (n = 3) show altered morphology, becoming multi-nucleated when compared to controls (Fig 2A $_{(1)}$ and $_{(2)}$). This is reflected in the measurements of filamentousness (Fig 2A $_{(5\text{-}7)}$ arbitrary units) where significant decreases in texture intensity (4.4 ± 0.47 vs 2.2 ± 0.03, $P<0.05$), fibre spot count (16.4 ± 0.64 vs 10.7 ± 2.1, $P<0.01$), fibre spot total area (1368 ± 51 vs

555 ± 23, P=0.0005) as well as cell count per well were observed (646 ± 186 vs 288 ± 103, P<0.05, Fig 2A $_{(3)}$) A significant increase in Krt 8 mean total fluorescence intensity (202632 ± 60337 vs 97262 ± 23343, P<0.05, arbitrary units, Fig 2A $_{(4)}$) was observed when comparing treated cells to controls. Acceptable Z'values (Fig 2B) were obtained for fibre spot count (0.95) and fibre spot total area (0.73), demonstrating suitability for high throughput development (Fig 2B).

Two further treatments affecting intermediate filaments; sodium butyrate and cordycepin, are assayable using the described methods.

Following 16 hours treatment with 20 mM sodium butyrate (n = 20), cells showed similar morphology, with contrast between the cytoplasm and the nuclear staining more pronounced when compared to untreated cells. 20 mM butyrate (Fig 3A $_{(3-5)}$) significantly reduced texture intensity (3.06 ± 0.38 vs 2.41 ± 0.39, P< 0.001), fibre spot count (5.78 ±0.85 vs 5.23 ± 0.6, P<0.02) and fibre spot total area (144.8 ± 11.8 vs 134.9 ± 8.3, P<0.005, all arbitrary units, paired students T test). A non-significant reduction in cell count per well was observed when comparing control to treated cells (670 ± 171 vs 627 ± 50, Fig 3A $_{(1)}$) emphasising the suitability of butyrate as a depolymerising agent without causing a disruption in cell number. As with griseofulvin, an increase in mean total Krt 8 fluorescence intensity was observed, though this was not significant (161983 ± 51982 vs 165148 ± 42567, arbitrary units, Fig 3A $_{(2)}$). Higher concentrations may be required to cause sufficient depolymerisation prior to cell death.

Visual inspection of cells treated for 15 minutes with 60 µM cordycepin (n = 3) confirmed that keratin fibres do retract to form a peri-nuclear ring, as observed by its effects on microtubules (Zieve et al [4]). This may explain the significant decrease in mean total Krt 8 fluorescence intensity (arbitrary units, Fig 3B $_{(2)}$) from 385698 ± 9862 vs 353452 ± 3297, P<0.05, in contrast to the increase observed with griseofulvin, P<0.05, and sodium butyrate (not significant). As with griseofulvin and sodium butyrate, texture intensity was also significantly decreased (Fig 3B $_{(3)}$, 2.39 ± 0.18 vs 1.57 ± 0.07, P<0.05, arbitrary units) indicating depolymerisation and a loss of filamentouness when compared to controls, though no significant differences were observed for measurements of fibre spot count (Fig 3B $_{(4)}$, 10.39 ± 1.15 vs 11.23 ± 1.98), fibre spot total area (Fig 3B $_{(5)}$, 733 ± 13 vs 653 ± 70, arbitrary units) and cell count per well (Fig 3B $_{(1)}$, 124 ± 12 vs 145 ± 60) when comparing controls to treated cells. This could possibly be attributed to the shorter treatment time with cordycepin (15 minutes) compared to griseofulvin (48

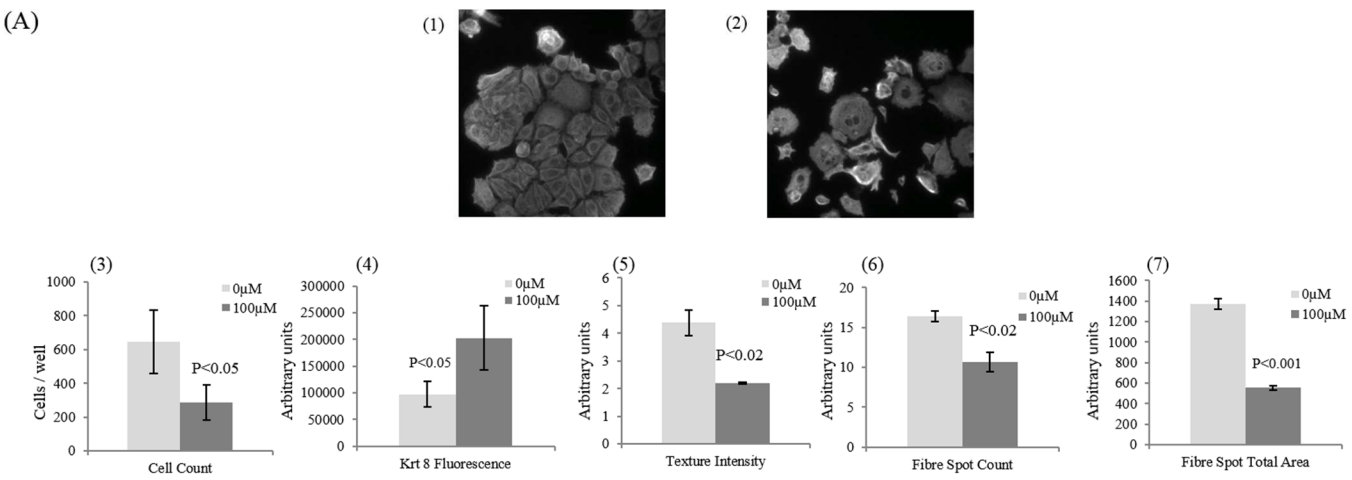

(B)

Treatment	Statistical Test	Cell Count	Krt 8 Fluorescence	Texture Intensity	Fibre Spot Count	Fibre Spot Total Area
Griseofulvin 0 v 100µM n = 3	Z-Prime	-1.42	-1.38	0.32	0.95*	0.73*
	Paired T-Test	0.024†	0.046†	0.015†	0.012†	0.0005†

Figure 2. *Assay Development and proof of Principle.* (A) Effect of Griseofulvin (n =3) on indicators of intermediate filament staining (arbitrary units). (1) PBS control 48h, x20 magnification, (2) 100µM Griseofulvin 48h, x20 magnification, (3) Cell count per well, (4) Mean total Krt 8 Fluorescence, (5) Texture Intensity, (6) Fibre spot count and (7) Fibre spot total area. (B) Statistical analysis of 0µM vs 100µM treatment using a Z prime calculation and paired students T-test. *Z prime values between 0.5 and 1 indicate suitability for high throughput development. †P values <0.05 are statistically significant.

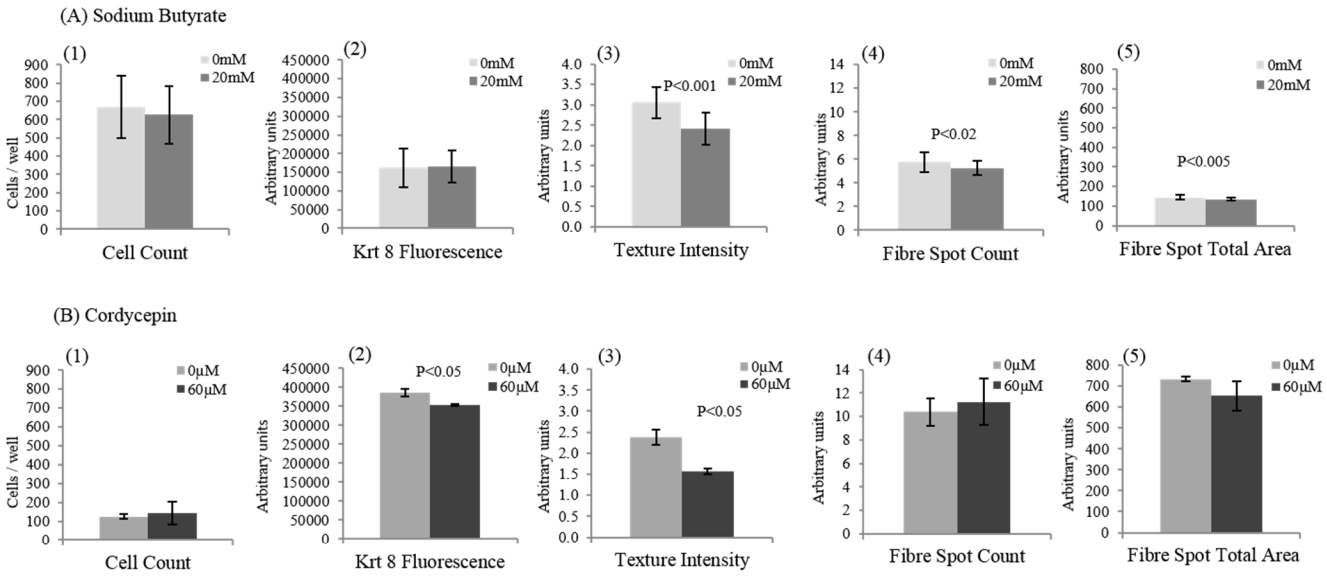

Treatment	Statistical Test	Cell Count	Krt 8 Flourescence	Texture Intensity	Fibre Spot Count	Fibre Spot Total Area
Sodium Butyrate (n=20)	Paired T-Test	0.2	0.8	0.001*	0.0156*	0.00336*
Cordycepin (n=3)	Paired T-Test	0.57	0.04*	0.025*	0.64	0.16

Figure 3. *Application of assay to demonstrate proof of principle.* A1 - A5; Sodium Butyrate, 16h, n = 20 and B1 – B5; Cordycepin, 15min, n = 3. Measurements for cell count per well (A1) and (B1) showed no significant difference when comparing control PBS treated cells to respective treatment. Significant decreases for indicators of intermediate filament staining (arbitrary units) were observed in butyrate treated cells for (A3) Texture intensity, (A4) Fibre spot count and (A5) Fibre spot total area, P<0.001, P<0.02 and P<0.005 respectively. Cells treated with cordycepin showed a significant decrease (P<0.05) in mean total Krt 8 fluorescence (B2) and texture intensity (B3).

hours) and sodium butyrate (16 hours) leading to a lower overall cell population by the end of the experiment (higher cordycepin doses around 200μM have been found to affect cell adhesion [26]).

The results indicate that a functional assay for the direct assessment of IF-perturbing drugs has been developed, optimised by the directed and informed combination of existing technologies. Keratins are emerging as potentially important targets in colorectal pathologies [7] and therefore may become the target for development of new therapeutics. As such, assays need to be in place for such applications. General cytoskeletal biology indicates that the various cytoskeletons are interlinked and collapse of one may impact upon another [4, 14, 15, 16]. This assay has the potential to be combined with a chemical stain (phalloidin) or antibody from another species to form a duplex or triplex assay for integrity of the microtubular, microfilamentous and IF cytoskeletons and thereby determine hierarchicality of impact of chemotherapeutics at the cellular level.

Acknowledgements

This work was funded by the Knowledge Transfer Partnership from the University of Sheffield.

References

[1] B. Alberts, A. Johnson, J. Lewis, M. Raff, How cells regulate their cytoskeletal filaments, in: Molecular Biology of the Cell, 2008, pp. 992 – 1009.

[2] T.M. Magin, P. Vijayaraj, R.E. Leube, Exp Cell Res, 313 (2007) 2021-2032. doi: 10.1016/j.yexcr.2007.03.005

[3] G.Z. Tao, D.M. Toivola, Q. Zhou, P. Strnad, B. Xu, S.A. Michie, M.B. Omary, J Cell Sci, 119 (2006) 1425-1432. doi: 10.1242/jcs.02861

[4] R. Windoffer, M. Beil, T.M. Magin, R.E. Leube, J Cell Biol, 194 (2011) 669-678. doi: 10.1083/jcb.201008095

[5] R. Moll, W.W. Franke, D.L. Schiller, B. Geiger, R. Krepler, Cell, 31 (1982) 11-24. doi: 10.1016/0092-8674(82)90400-7

[6] S.H. Leech, C.A. Evans, L. Shaw, C.H. Wong, J. Connolly, J.R. Griffiths, A.D. Whetton, B.M. Corfe, Proteomics, 8 (2008) 279-288. doi: 10.1002/pmic.200700404

[7] D. Majumdar, J.P. Tiernan, A.J. Lobo, C.A. Evans, B.M. Corfe, Int J Exp Pathol, 93 (2012) 305-318. doi: 10.1111/j.1365-2613.2012.00830.x

[8] P.J. Drake, G.J. Griffiths, L. Shaw, R.P. Benson, B.M. Corfe, J Proteome Res, 8 (2009) 28-34. doi: 10.1021/pr8006396

[9] B.M. Corfe, A.Q. Khan, L. Shaw, P.J.M. Drake, G.J. Griffiths,

S.R. Brown, Journal of Integrated OMICS, 1 (2011). doi: 10.5584/jiomics.v1i2.57

[10] J. Kilner, B.M. Corfe, S.J. Wilkinson, Mol Biosyst, 7 (2011) 975-983. doi: 10.1039/c0mb00281j

[11] M.B. Omary, P.A. Coulombe, Intermediate Filament Cytoskeleton, in: Methods in Cell Biology, 2004, pp. 1-886.

[12] R. Windoffer, R.E. Leube, Cell Motil Cytoskeleton, 50 (2001) 33-44. doi: 10.1002/cm.1039

[13] W.E. Gordon, A. Bushnell, K. Burridge, Cell, 13 (1978) 249-261. doi: 10.1016/0092-8674(78)90194-0

[14] L.W. Knapp, W.M. O'Guin, R.H. Sawyer, J Cell Biol, 97 (1983) 1788-1794. doi: 10.1083/jcb.97.6.1788

[15] S. Woll, R. Windoffer, R.E. Leube, Eur J Cell Biol, 84 (2005) 311-328. doi: 10.1016/j.ejcb.2004.12.004

[16] E. Drouhet, B. Dupont, Rev Infect Dis, 9 Suppl 1 (1987) S4-14. doi: 10.1093/clinids/9.Supplement_1.S4

[17] H. Salmhofer, I. Rainer, K. Zatloukal, H. Denk, Hepatology, 20 (1994) 731-740. doi: 10.1002/hep.1840200326

[18] B. Rebacz, T.O. Larsen, M.H. Clausen, M.H. Ronnest, H. Loffler, A.D. Ho, A. Kramer, Cancer Res, 67 (2007) 6342-6350. doi: 10.1158/0008-5472.CAN-07-0663

[19] K. Rathinasamy, B. Jindal, J. Asthana, P. Singh, P.V. Balaji, D. Panda, BMC Cancer, 10 (2010) 213. doi: 10.1186/1471-2407-10-213

[20] K.G. Cunningham, W. Manson, F.S. Spring, S.A. Hutchinson, Nature, 166 (1950) 949. doi: 10.1038/166949a0

[21] G.W. Zieve, E.J. Roemer, Exp Cell Res, 177 (1988) 19-26. doi: 10.1016/0014-4827(88)90021-3

[22] H. Thomadaki, A. Scorilas, C.M. Tsiapalis, M. Havredaki, Cancer Chemother Pharmacol, 61 (2008) 251-265. doi: 10.1007/s00280-007-0467-y

[23] W.C. Wu, J.R. Hsiao, Y.Y. Lian, C.Y. Lin, B.M. Huang, Cancer Chemother Pharmacol, 60 (2007) 103-111. doi: 10.1007/s00280-006-0354-y

[24] Y.Y. Wong, A. Moon, R. Duffin, A. Barthet-Barateig, H.A. Meijer, M.J. Clemens, C.H. de Moor, J Biol Chem, 285 (2010) 2610-2621. doi: 10.1074/jbc.M109.071159

[25] S. Choi, M.H. Lim, K.M. Kim, B.H. Jeon, W.O. Song, T.W. Kim, Toxicol Appl Pharmacol, 257 (2011) 165-173. doi: 10.1016/j.taap.2011.08.030

[26] W. Scheppach, H.P. Bartram, F. Richter, Eur J Cancer, 31 (1995) 1077-1080. doi: 10.1016/0959-8049(95)00165-f

[27] J.P. Whitlock, Jr., D. Galeazzi, H. Schulman, J Biol Chem, 258 (1983) 1299-1304.

[28] J.H. Zhang, Journal of Biomolecular Screening, 4 (1999) 67-73. doi: 10.1177/108705719900400206